

Numerical simulation of Permafrost Depth in the Netherlands

Joan Govaerts, Koen Beerten, Johan ten Veen

**Report in the framework of the OPERA2
project, WP 4, task 4.1.2
(contract OPERA-RP-TNO412)**

March, 2015

IPA
SCK•CEN
Boeretang 200
BE-2400 Mol
Belgium

PAS

Distribution list

Name	Expert Group	Number
Johan ten Veen	TNO	3
Joan Govaerts	SCK•CEN	1
Koen Beerten	SCK•CEN	1
Mieke De Craen	SCK•CEN	1

		Date	Approval
Author:	Joan Govaerts	13/3/2015	
Verified by:	Koen Beerten	13/03/2015	
QA-verification:	Elke Jacobs	16/03/2015	^{io} 
Approved by:	Mieke De Craen	2015-03-13	

RESTRICTED

All property rights and copyright are reserved. Any communication or reproduction of this document, and any communication or use of its content without explicit authorization is prohibited. Any infringement to this rule is illegal and entitles to claim damages from the infringer, without prejudice to any other right in case of granting a patent or registration in the field of intellectual property.

SCK•CEN, Studiecentrum voor Kernenergie/Centre d'Etude de l'Energie Nucléaire
Stichting van Openbaar Nut – Fondation d'Utilité Publique - Foundation of Public Utility
Registered Office: Avenue Herrmann Debroux 40 – BE-1160 BRUSSEL
Operational Office: Boeretang 200 – BE-2400 MOL

Numerical simulation of Permafrost Depth in the Netherlands

Joan Govaerts, Koen Beerten, Johan ten Veen

**Report in the framework of the OPERA2
project, WP 4, task 4.1.2
(contract OPERA-RP-TNO412)**

March, 2015
Status: Confidential

IPA
SCK•CEN
Boeretang 200
BE-2400 Mol
Belgium

PAS

Table of Contents

1. Introduction.....	7
2. Objectives, research task and strategy	7
3. Mathematical and numerical model for permafrost growth and degradation.....	9
3.1. Frozen soil physics	9
3.2. Equivalent heat capacity	10
3.3. Heat conductivity.....	11
3.4. Implementation in COMSOL multiphysics.....	11
3.5. Parameters, initial and boundary conditions used in the reference calculation.....	12
3.5.1. Parameters: Porosity, lithology and overburden	12
3.5.2. Initial condition	16
3.5.3. Upper boundary condition: temperature evolution of a future glacial cycle.....	16
3.5.4. Lower boundary condition: geothermal flux.....	20
4. Stochastic uncertainty and sensitivity analysis	23
4.1. Classification of uncertainties	23
4.2. Uncertainty Analysis (UA).....	24
4.2.1. Monte Carlo simulation using Latin Hypercube Sampling.....	24
4.2.2. Implementation.....	26
4.2.3. Parameter Ranges	26
4.3. Sensitivity analysis	27
4.3.1. Standardized Regression Coefficients.....	28
4.3.2. Correlation coefficients	29
5. Results	30
5.1. Permafrost development during a Weichselian temperature cycle – reference case.....	30
5.2. Interpolated best estimate maximum permafrost depth maps - reference case	32
5.3. Results of the uncertainty analysis	36
5.4. Results of the sensitivity analysis.....	37
6. Conclusions	42
7. References	43

1. Introduction

The Rupelian clay in the Netherlands is currently being the subject of a feasibility study with respect to the storage of radioactive waste in the Netherlands (OPERA-project). Many features need to be considered in the assessment of the long-term evolution of the natural environment surrounding a geological waste disposal facility. One of these is permafrost development, as climate simulations indicate the return of glacial and periglacial conditions in northwestern Europe at some point during the next one hundred thousand years and more (BIOCLIM, 2001), and given the presence of geological remnants of permafrost induced soil deformation at the surface (Beerten, 2011). Whereas the surficial lateral extent, type and timing of frozen ground in the past is, generally speaking, relatively well known in Belgium and the Netherlands from periglacial deformation phenomena, the maximum depth of permafrost development is difficult to observe in the geological record. Therefore, numerical simulation seems to be the most suitable tool to estimate permafrost depth, and has been applied already in several case studies elsewhere in Europe (Govaerts et al., 2011).

Permafrost development may have a significant impact on various components of the disposal system, including the natural environment and engineered barrier. The hydrological cycle will completely change under permafrost conditions, up to the point where surface and subsurface hydrology become completely independent, and groundwater flow is reduced to near-zero. Hydraulic properties of aquifer sands and aquitard clays might be affected during permafrost, especially if it is accompanied by repeated freeze-thaw cycles. Finally, the rate of thermodynamic processes will be altered significantly with changing temperatures, as will microbial activity in the underground.

As the future climate is impossible to predict, the strategy for future permafrost simulation is based on past analogies. The Weichselian glacial is usually taken as an analogue for the future, and reconstructed temperatures for this glacial are then thought to be representative for a future glacial cycle somewhere during the next several hundred thousands of years. Obviously, palaeoclimatic indicators are much better preserved for the last glacial than previous glacials.

The aim of this report is to present permafrost depth calculations for well-defined areas in the Netherlands that are representative for a specific geological setting (depth of the Rupelian clay, thickness and type of overburden, porosity, geothermal flux, etc.), using a best estimate temperature curve for a glacial cycle. In addition, results from the uncertainty analysis will be presented that give an indication of the probability of nation-wide permafrost depths under a future glacial climate, taking into account various combinations of temperature, overburden lithology, porosity and geothermal flux. Subsequently, a sensitivity analysis is performed to identify the parameters that are the most important. Finally, the results will be discussed in the light of previous permafrost calculations for other regions in Europe.

2. Objectives, research task and strategy

The objective of the study is to generate permafrost depth estimates under a future glacial climate for the entire Dutch territory. Permafrost development is dependent on atmospheric and surface boundary conditions, basically temperature and vegetation, and subsurface properties such as lithology, porosity and geothermal flux. As such, it is the result of interactions between global changes (temperature) and local conditions (subsurface geology). The research task and strategy

adopted for this specific study consists of the following elements. First, we try to simulate a future glacial climate using the Weichselian glaciation (115-11 ka BP) as an analogue. Various temperature estimates are available for this glacial period, many of them being derived from palaeoclimatological archives in the Netherlands. The input temperature is held constant for the entire country. Subsequently it will be used to force the subsurface model, which is fragmented into different representative polygons.

The depth of structural subsurface units (affecting porosity and therefore the effective thermal properties) and their lithofacies distribution (affecting the average porosity of the unit) are considered relevant for permafrost modelling. Note that the depth to the top Rupel Fm. is representative for the total overburden depth, which is strongly affected by thick units such as the Breda Fm. The thickness distribution of the latter is strongly coupled to the tectonic setting, i.e., thick in basins and relatively thin in structural highs. Also lithofacies (given as % of clay or sand) seems to be linked to certain structural elements, especially in the Roer Valley Graben (RVG). In the north this correlation is less obvious. Area selection for permafrost modelling is based on the presence of 17 structural elements, including 6 highs, 5 basins and 6 platforms.

Subsequently, a geological (property) model was constructed based on the surfaces of the DGM shallow subsurface model. For each unit, vertical gridcells with a height equal to unit thickness of 250x250m were constructed. These gridcells were populated with the parameters described before. Subsequently, all parameters were averaged over the vertical interval overlying the Rupel Fm. (the overburden).

The research area is subdivided into several polygons which dimensions range roughly between 9x15km and 110x140km. Details about the midpoint positions and exact dimensions of the various polygons is given in Table 1 while the midpoints are plotted in Figure 1.

Table 1 – RD-coordinates of the midpoints of the various polygons, as well as the polygon dimensions (Δ) and latitudinal and longitudinal position.

Polygon	X (m)	Y (m)	ΔX (m)	ΔY (m)	Lat.	Long.
CNB	179625	478875	99500	85000	52°17'54"	05°44'22"
DRH	225000	494625	92250	88750	52°26'09"	06°25'02"
FPwest	129000	570500	164750	103750	53°07'18"	04°59'55"
FRP	176625	555000	54750	64000	52°58'58"	05°42'26"
GRP	222250	549000	51500	38500	52°55'31"	06°23'15"
KempH	140500	373000	114750	79750	51°20'49"	05°10'45"
LBH	191625	331375	24250	26250	50°58'18"	05°54'33"
LSB	248875	546000	13500	17500	52°53'39"	06°46'58"
NHP	133125	527250	80250	73250	52°44'00"	05°03'35"
OHP	112625	399750	20250	38500	51°35'10"	04°46'02"
PMC	175250	417125	9500	15250	51°44'36"	05°40'42"
PMC zuid	202875	369750	111000	141000	51°18'57"	06°04'28"
RVG	158375	383625	74000	106250	51°26'33"	05°25'51"
TIJH	149625	539875	89250	71000	52°50'50"	05°18'10"
VLB	144250	578500	22000	21500	53°11'39"	05°13'28"
WNB	110000	447500	73250	105500	52°00'54"	04°43'13"
ZH	73125	400875	57250	50500	51°35'31"	04°11'34"

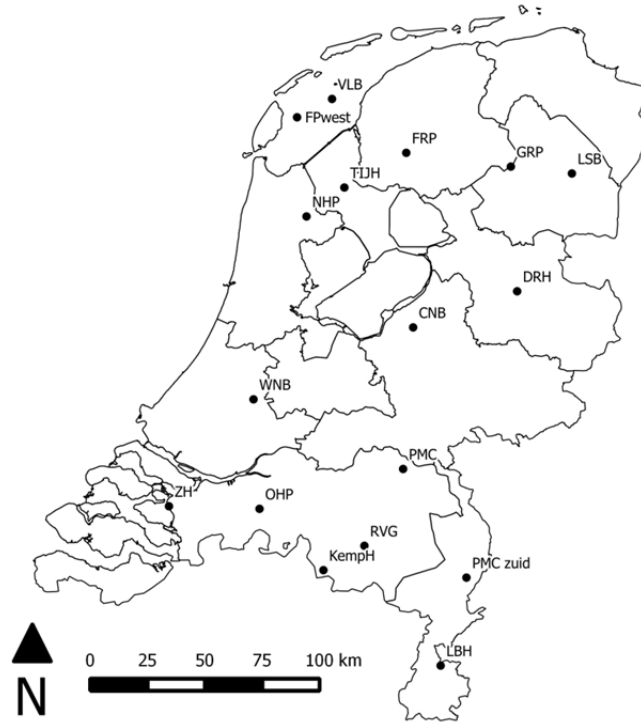


Figure 1 – Polygon midpoints plotted on administrative map of the Netherlands.

3. Mathematical and numerical model for permafrost growth and degradation

3.1. Frozen soil physics

To describe heat transport in the subsoil of the Netherlands, the following one-dimensional enthalpy conservation equation is used with heat transport only occurring by conduction.

$$C_{eq} \frac{\partial T}{\partial t} + \nabla \cdot (-\lambda_{eq} \nabla T) = Q \quad (1)$$

where C_{eq} is the effective volumetric heat capacity ($J/K \cdot m^3$), T is temperature (K), λ_{eq} is the effective thermal conductivity ($W/m \cdot K$), and Q is a heat source (W/m^3).

When modelling the thermal effects of freezing and thawing, equation (3.1) has to include three phases: rock matrix, fluid and ice. To achieve this, the following volume fractions are defined:

$$\theta_m = 1 - \theta, \quad \theta_f = \theta \cdot \Theta, \quad \theta_i = \theta - \theta_f \quad (2)$$

The subscripts f , i and m account for the mixture between solid rock matrix (m), fluid-filled pore space (f) and ice filled pore space (i). This mixture is characterized by porosity θ and Θ denotes the

fraction of pore space occupied by fluid. As a result of the complicated processes in the porous medium, melting cannot be considered as a simple discontinuity. Θ is generally assumed to be a continuous function of temperature in a specified interval (see 3.4).

3.2. Equivalent heat capacity

When a material changes phase, for instance from solid to liquid, energy is added to the solid. This energy is the latent heat of phase change. Instead of creating a temperature rise, the energy alters the material's molecular structure. This latent heat of freezing/melting of water, L , is 333.6 kJ/kg (Mottaghy & Rath, 2006) which is more than one order of magnitude larger than the value used by Walravens (1996). C_{eq} is a volume average, which also accounts for the latent heat of fusion:

$$C_{eq} = \theta_m \rho_m c_m + \theta_f \rho_f \left(c_f + \frac{\partial \Theta}{\partial T} L \right) + \theta_i \rho_i \left(c_i + \frac{\partial \Theta}{\partial T} L \right) \quad (3)$$

where ϑ is the volumetric content, ρ equals density (kg/m³), and c is the specific heat capacity (J/(K·kg)). It includes additional energy sources and sinks due to freezing/melting using the latent heat of fusion L for only the normalized pulse around a temperature transition $\frac{\partial \Theta}{\partial T}$ (K⁻¹). The

integral of $\frac{\partial \Theta}{\partial T}$ must equal unity to satisfy the condition that pulse width denotes the range between the liquidus and solidus¹ temperatures. This approach is similar to the one used by Mottaghy & Rath (2006), Bense et al. (2009), Noetzli & Gruber (2009), Holmén et al. (2011) and Kitover et al. (2013). Values for the porosity, density and specific heat of the different components are given in Table 2.

Table 2: Properties of the different components of the subsoil

Parameter	Water	Ice	Boom Clay Matrix	Sand Matrix
Density [kg/m ³]	997	918	2803	2358
Porosity	-	-	0.39	From TNO data sheet
Specific Heat [J/(kg K)]	4185	1835	820	800
Thermal conductivity [W/(m K)]	0.54	2.37	1.98 ²	3.00

The values of the specific heat of the Boom Clay matrix are obtained from the ATLAS study (Cheng et al., 2010). The equivalent heat capacity then adds up to 1443 J/(kg K) and 981 J/(kg K) for the fully unfrozen and frozen state respectively. This is in the same range as the values used by Walravens,

¹ During heating, solidus is that temperature at which a solid begins to melt. Between the solidus and liquidus temperatures, there will be a mixture of solid and liquid phases. Just above the solidus temperature, the mixture will be mostly solid with some liquid phases. Just below the liquidus temperature, the mixture will be mostly liquid with some solid phases.

² This value has been chosen so the effective thermal conductivity equals 1.31 J/(kg K), which is the vertical thermal conductivity of Boom Clay obtained during the ATLAS study.

1400 and 960 J/(kg K), (Marivoet & Bonne, 1988) and Kömle et al. (2007), 1266 and 977 J/(kg K) for clay sediments.

The value of the sand matrix is set to a value inside the ranges which are found for quartz minerals and sands (see Mallants, 2006 and references therein). For sandy soils, the equivalent heat capacity adds up to 1319 J/(kg K) and 937 J/(kg K) for the fully unfrozen and frozen state respectively when a porosity of 30% is assumed.

3.3. Heat conductivity

In case of a phase change at a single temperature, thermal conductivity is not continuous with respect to temperature. However, considering the freezing range in rocks, we use equation (1) and (2) for taking into account the contributions of the fluid and the ice phase. Since the materials are assumed to be randomly distributed, the weighting between them is realized by the square-root mean, which is believed to have a greater physical basis than the geometric mean (Mottaghy & Rath, 2006).

$$\lambda_{eq} = \left(\theta_m \sqrt{\lambda_m} + \theta_f \sqrt{\lambda_f} + \theta_i \sqrt{\lambda_i} \right)^2 \quad (4)$$

Values for the thermal conductivity of the different components are given in Table 2.

The values of the thermal conductivity of the rock matrix of Boom clay and sand are chosen in the same order of magnitude of the values used by Bense et al. (2009) and Mottaghy & Rath (2006), who used respectively 4.0 W/(m K) and 2.9 W/(m K) for a generic sediment rock species.

For Boom clay, the equivalent thermal conductivity then adds up to 1.31 J/(kg K) and 2.03 J/(kg K) for the fully unfrozen and frozen state respectively. The conductivity value of unfrozen Boom Clay is thus equal to the vertical conductivity obtained from the ATLAS 3 study (Cheng et al., 2010).

In sandy soils, the equivalent thermal conductivity is 2.05 W/(m K) and 2.80 W/(m K) for the fully unfrozen and frozen state respectively. The values are in the same range as the values found in Mallants (2006) and references therein. The value for the frozen state is significantly lower than the one used by Walravens (3.60 J/(kg K)).

3.4. Implementation in COMSOL multiphysics.

The heat transport equation is implemented in COMSOL multiphysics, Earth Science Module (2008), together with all the correlations for the thermal properties. Because the thermal properties differ between the frozen and unfrozen state, a variable Θ is created, which goes from unity to zero for fully unfrozen to frozen. Therefore, the effective properties switch with the phase through multiplication with Θ .

The switch in Θ from 0 to 1 occurs over the liquid-to-solid interval (0.5°C to -0.5°C) using a smoothed Heaviside function to ensure numerical stability. The model implements the Heaviside function with the expression $\Theta = \text{flc2hs}(T-T_{\text{trans}},dT)$; where the transition temperature is T_{trans} and the transition interval for the function is dT , which is set to 1K. The pulse is the derivative of Θ with respect to

temperature. $\frac{\partial \Theta}{\partial T}$ is expressed with the COMSOL Multiphysics differentiation operator, d. The sensitivity of the results to the width of the liquid-to-solid interval is investigated in appendix A.

3.5. Parameters, initial and boundary conditions used in the reference calculation

The reference calculation consists of 17 simulations of permafrost pro- and degradation during a Weichelian cycle. Each calculation is performed for one of the seventeen polygons described in section 2 using best estimate parameter values, initial and boundary conditions. These are discussed in more detail in the following section.

3.5.1. Parameters: Porosity, lithology and overburden

One of the necessary parameters in modelling of permafrost depth is porosity. Here, we aim to assign a porosity value to each of the lithostratigraphic units defined in the Digital Geological Model (DGM) of the shallow Dutch subsurface. The hydrogeological model REGIS provides a further subdivision and includes both aquifers (sand) and non-aquifer layers (clay). Using the REGIS information a percentage of clay vs. sand for each of the DGM units can be calculated. Given the relatively small amount of porosity measurements of the sand and clay layers in the stratigraphic interval above the Rupel Fm., a best fit, generally applicable, porosity-depth relationship was established (using Petromod functionality) for all units based on the available measurements. This allows to make porosity predictions in non-studied domains. For those units without any measurement the porosity was determined using the relationship of the depositional facies.

Several trends can be observed from Figure 2. The highest averaged mid-depth porosities for the post-Rupelian overburden are observed in the east and the southwest, reaching 50%. The lowest values are found in the southeast (Roer Valley Graben, polygon RVG) and the northwest. The porosity is basically influenced by two other parameters: lithology and burial depth (Figure 3 and Figure 4). The thicker the post-Rupelian overburden, the deeper the mid-depth for which the porosity is determined, and thus the lower the porosity. Lithology also has an influence on porosity because on average, clay has a higher porosity than sand. As such, the porosity map is a mirror image of a combination of lithology and overburden thickness.

Table 3 – Mid-depth porosity for the different polygons (%). Minimum (min) and maximum (max) values in the dataset are given, as well as the range (Δ), mean, standard deviation (σ) and number of observations.

Polygon	min	max	Δ	mean	σ	n
CNB	0	71	71	42	8	127554
DRH	36	59	23	51	3	1384
FPwest	41	43	2	42	0	2274
FRP	23	48	24	43	2	56414
GRP	0	70	70	46	5	105484
KempH	12	55	43	48	4	1709
LBH	6	77	72	45	7	4223
LSB	23	58	35	47	3	30397
NHP	39	45	6	42	1	16365
OHP	42	55	13	50	2	15792
PMC	21	71	50	47	5	42245
PMC zuid	34	69	35	44	3	3816
RVG	36	61	24	41	3	46186
TIJH	27	44	17	42	1	34685
VLB	26	45	19	41	1	18336
WNB	24	52	28	44	2	67433
ZH	0	67	67	48	9	53241

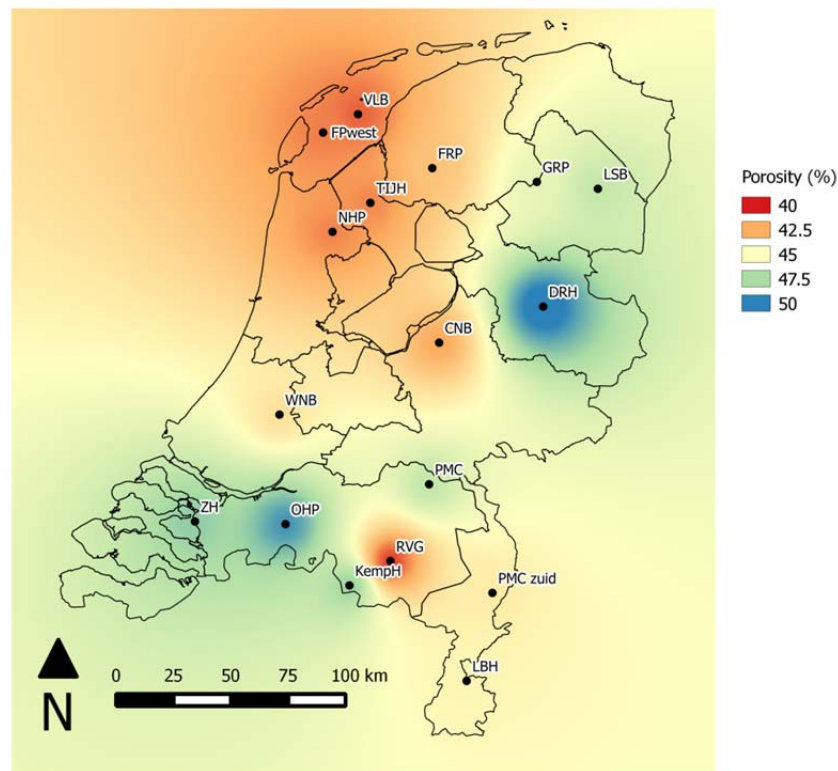


Figure 2 – Averaged mid-depth porosity variability of the post-Rupelian overburden.

Table 4 – Sand content (%). Minimum (min) and maximum (max) values in the dataset are given, as well as the range (Δ), mean, standard deviation (σ) and number of observations.

Polygon	min	max	Δ	mean	σ	n
CNB	0	100	100	65	25	127557
DRH	42	80	38	64	7	1384
FPwest	50	78	28	75	2	2274
FRP	28	99	71	69	13	56414
GRP	0	100	100	52	21	105673
KempH	20	98	78	62	18	1709
LBH	0	100	100	92	15	4223
LSB	12	100	88	54	14	30397
NHP	54	90	36	80	5	16365
OHP	33	100	67	72	12	15792
PMC	0	100	100	66	32	42245
PMC zuid	60	100	40	99	3	3818
RVG	6	100	94	91	14	46186
TIJH	47	90	43	79	6	34685
VLB	37	80	43	69	6	18338
WNB	16	99	83	74	12	67436
ZH	0	100	100	75	20	53251

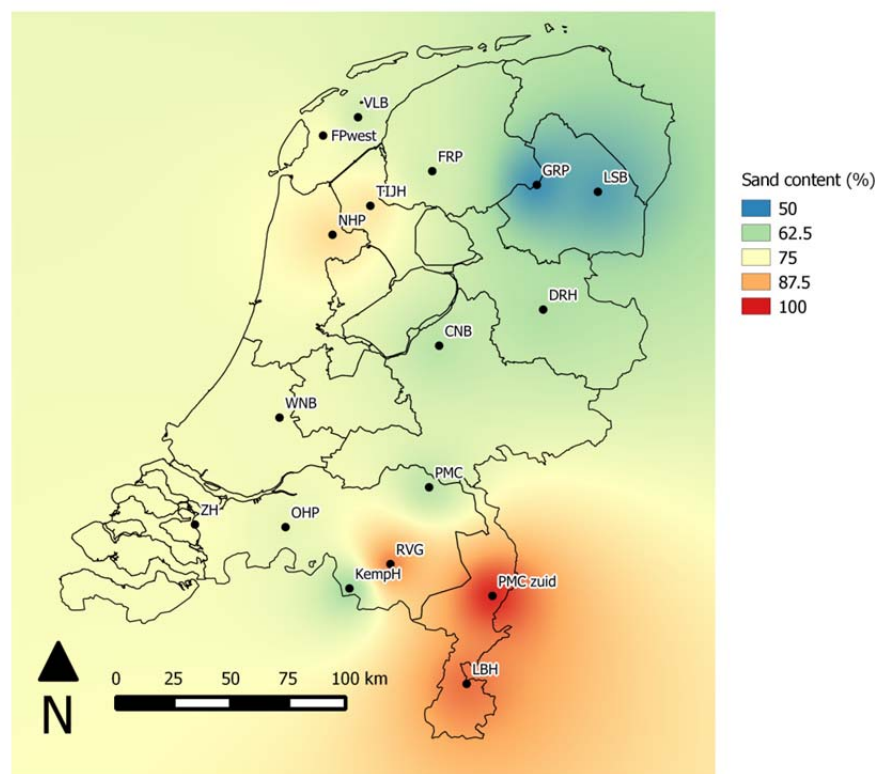


Figure 3 – Distribution of the average sand content in the post-Rupelian overburden.

Table 5 – Depth of the top of the Rupel Formation (m). Minimum (min) and maximum (max) values in the dataset are given, as well as the range (Δ), mean, standard deviation (σ) and number of observations.

Polygon	min	max	Δ	mean	σ	n
CNB	21	1213	1192	656	317	127563
DRH	148	284	136	203	31	1384
FPwest	654	791	137	730	26	2274
FRP	340	842	502	546	91	56414
GRP	22	744	722	360	136	105383
KempH	275	617	342	458	94	1709
LBH	31	937	906	280	274	4228
LSB	85	520	435	233	64	30397
NHP	626	1029	403	801	81	16365
OHP	215	674	458	356	91	15792
PMC	102	1167	1065	409	159	42246
PMC zuid	55	1047	993	423	153	3818
RVG	266	1559	1293	1034	294	46186
TIJH	515	884	369	684	61	34685
VLB	541	834	294	710	59	18338
WNB	281	1084	803	559	167	67436
ZH	7	428	421	172	72	53259

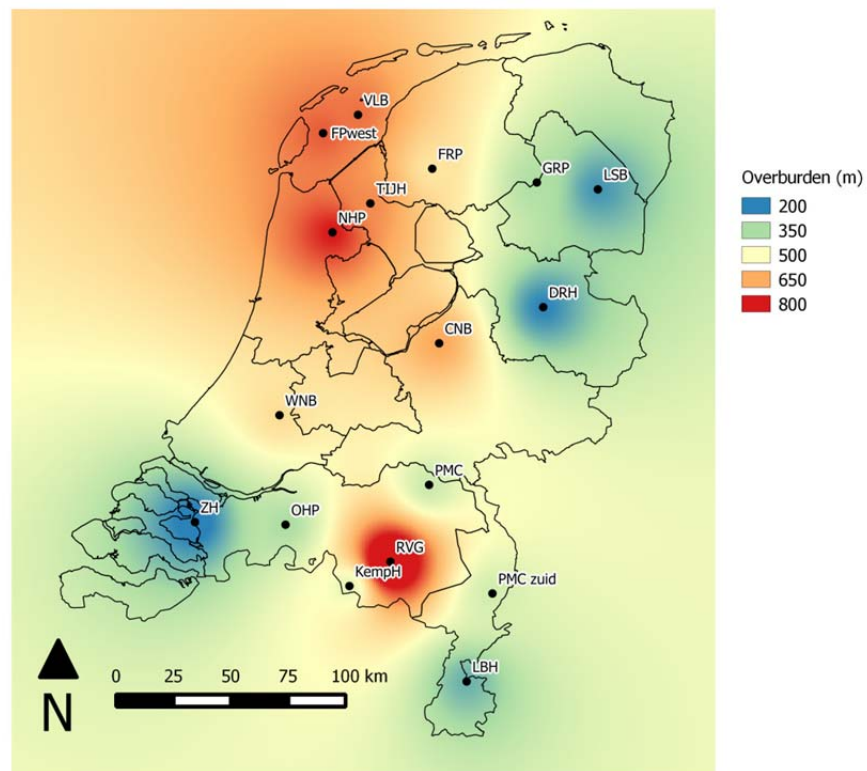


Figure 4 – Depth of the top of the Rupel Formation, also representing the thickness of the overburden (m).

3.5.2. Initial condition

It is assumed that the initial temperature profile at the start of the calculations, which is 120 000 years ago, is equal to present day conditions. The temperature profile is then calculated using the overburden thickness, the temperature gradient and the mid-depth temperature provided by TNO.

3.5.3. Upper boundary condition: temperature evolution of a future glacial cycle

The upper boundary condition is the temperature evolution of a future glacial cycle for which the Weichselian glacial is taken as an analogue. The temperature curve from Beerten (2011) and Govaerts et al. (2011) was significantly modified to include better estimates of the mean annual air temperature. Moreover, a minimum and maximum temperature curve was produced as input for stochastic simulations.

Palaeoclimatic and palaeoenvironmental evidence is preserved indirectly in biotic and abiotic records in sedimentary sequences (Huijzer and Vandenberghe, 1998). In the multiproxy approach for climate reconstruction, evidence of different origin is collected, analysed and synthesised, and converted into climate parameter values. Proxy data relevant to the reconstruction of the Weichselian climate include aeolian, fluvial and glacial deposits and/or landforms. Periglacial structures (frost cracks, cryoturbations, ice-wedge casts) are important abiotic proxy data within these sediments and are often the primary source of evidence. Botanical (pollen and plant macrofossils) and faunal evidence (beetles, ostracods, molluscs and vertebrates) are used as biotic proxy data from these deposits.

The temperature curves and data used in this study are shown in [Figure 5](#), [Figure 6](#) and [Table 6](#). Best estimates for the mean annual air temperature (MAAT) during isotope stage 5 is based on pollen data from van Gijssel (1995), but replotted against a more recent chronostratigraphical framework for the Weichselian glaciation (see Busschers et al., 2007, and references therein). The main features of the MIS5 climate (marine isotope stage 5) is the relatively mild stadials 5b and 5d, with an MAAT of -2°C , and the relatively cold interstadials 5c and 5a, with an MAAT of $+4^{\circ}\text{C}$. The first period with continuous permafrost development in the Netherlands is MIS4, with MAAT values dropping to as low as -4°C and even -8°C for the end of MIS4, based on periglacial deformation phenomena (Huijzer and Vandenberghe, 1998). The following MIS3 is characterised by a somewhat milder climate, showing less periglacial deformation of the subsoil. Analysis of flora and fauna preserved within MIS3 sediments, and the type and nature of periglacial deformation shows that some interstadials might have reached an MAAT between 0°C and $+6^{\circ}\text{C}$ (e.g., Upton Warren, Hengelo and Denekamp interstadials; Huijzer and Vandenberghe, 1998, Busschers et al., 2007 and van Gijssel, 1995), and several stadials would have reached an MAAT as low as -4°C (e.g., Hasselo stadial; Busschers et al., 2007). Subsequently, the climate evolves towards the Late Glacial Maximum, which is situated in MIS2. Data for this stage is mainly derived from Renssen and Vandenberghe (2003) and Buylaert et al. (2008), and is based on the presence and type of periglacial deformation phenomena. The MAAT for the period between 28 ka and 15 ka would not have exceeded 0°C , while some periods show MAAT values as low as -8°C to -9°C . Finally, the end of MIS2 is characterised by a stepwise trend towards global warming, reaching present-day MAAT values of around $+10^{\circ}\text{C}$ for MIS1.

Upper and lower bounds for these temperature data are given in [Figure 6](#) and [Table 6](#). They serve as input for the permafrost depth uncertainty analysis (see section 5.3). Instead of using one best

estimate temperature evolution for the Weichselian, a minimum and maximum temperature distribution for each period is used, which is randomly sampled to produce various combinations of upper and lower bound MAAT values. Different sources of uncertainty are thus taken into account, such as the reliability of the palaeotemperature proxy, the transferability towards a future glacial climatic cycle, temperature gradients across the country and atmosphere-soil temperature coupling, i.e. the influence of vegetation and snow cover which is not taken into account explicitly. This means that in any case, the lower bound is at least 2°C lower than the best estimate, unless lower values are given in one of the above quoted studies. For MIS4 and MIS2, lower bound values are set to -4°C for the warmer periods, and -8°C for the colder periods, except for the two coldest temperature intervals where MAAT is set to -10°C to -11°C. The reasoning behind this that permafrost would require an MAAT below -4°C for the discontinuous type and -8°C for the continuous type (see references in Beerten, 2011). Thus, for time intervals where discontinuous permafrost conditions have been reconstructed, the minimum bound is set to the threshold temperature for continuous permafrost. The same principle applies for time intervals where only sporadic permafrost has been observed. For MIS5, lower bound values are taken from van Gijssel (1995), while for MIS3 they are based on Huijzer and Vandenberghe (1998).

The upper bound is based on a warm solution of the Weichselian climate, which is reconstructed from a pollen sequence in sediments from the crater lake at La Pile (Guiot et al., 1989; in Busschers et al., 2007). Their mean estimate of the MAAT is used as an absolute maximum scenario for the Weichselian glacial and any future glacial cycle during the next one million years. The upper bound for the time period around 20 ka, for which the La Pile pollen record gives no solution, is set to -4°C, because permafrost appeared to be widespread during that time period in western Europe.

As already mentioned, the temperature data presented here are used as soil input data, without taking into account any buffering from vegetation or soil. This means that the best estimate permafrost calculations are in fact conservative estimates, whereas the influence from vegetation and snow is implicitly accounted for in the stochastic calculations. The upper bound is always a few degrees above the best estimate, and this higher temperature estimate would yield reasonable soil temperature estimates with snow and/or vegetation shielding.

Furthermore, the model is conservative as well with respect to the following phenomena. Firstly, vadose zone hydrology is neglected, but during very cold stadials, infiltration would probably be so low as to lower the groundwater table significantly. Next, groundwater flow is neglected as well, but it is evident that this would slow down the speed of permafrost development. Finally, outfreezing of pore water salt would lower the speed of permafrost development because more latent heat is needed to freeze water with elevated salt concentrations.

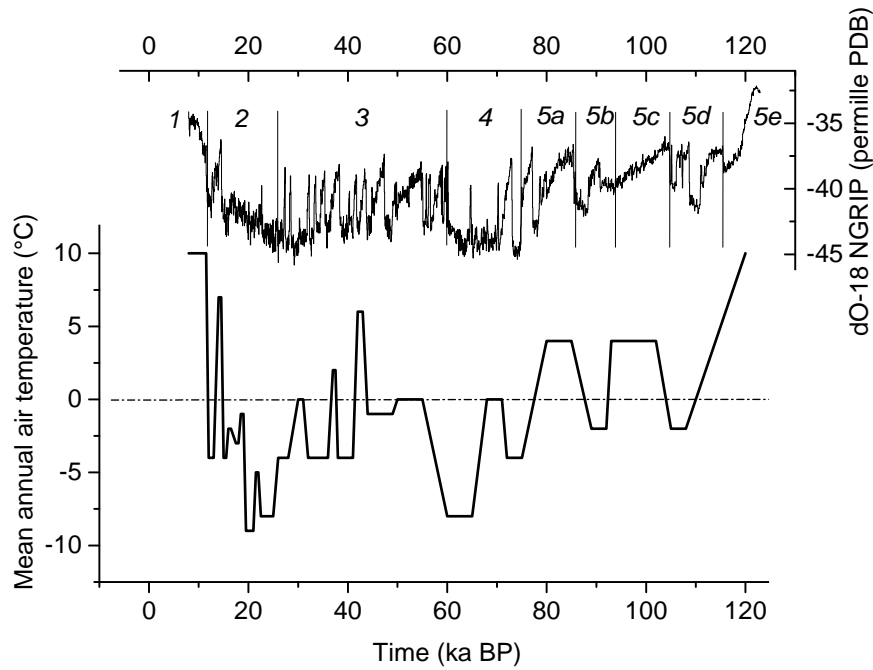


Figure 5 – Best estimate temperature evolution for the Weichselian glaciation, which is taken as an analogue for a future glacial climate in permafrost calculations. The curve is based on data from van Gijssel (1995), Huijzer and Vandenberghe (1998), Renssen and Vandenberghe (2003), Busschers et al. (2007) and Buylaert et al. (2008). Marine isotope stages (numbering 1 to 5e) are taken from Busschers et al. (2007) and references therein. The oxygen isotope curve is reproduced from NGRIP (2004) data.

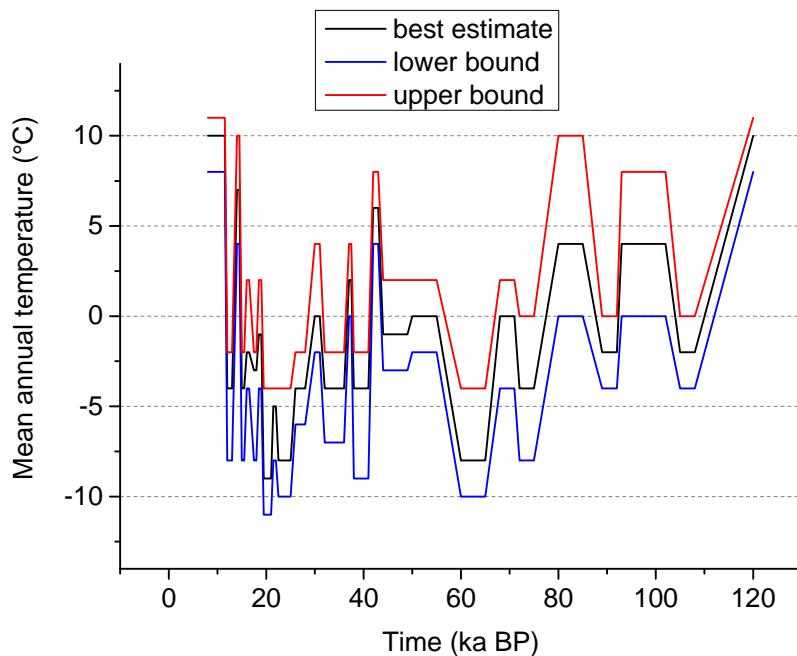


Figure 6 – Upper and lower bound values for stochastic permafrost calculations. Upper bound values are based on Guiot (1989) in Busschers et al. (2007) while lower bound values are based on threshold values for periglacial deformation types, and an overall 2°C envelope with respect to the best estimate.

Table 6 – Mean annual air temperature (MAAT) data for the Weichselian glacial: best estimate, minimum envelope and maximum envelope. Based on Guiot et al. (1989), van Gijssel (1995), Huijzer and Vandenberghe (1998), Renssen and Vandenberghe (2003), Busschers et al. (2007) and Buylaert et al. (2008). Several stadials and interstadials are explicitly mentioned (Upton Warren, Hasselo, Hengelo, Denekamp, LGM, Bölling-Alleröd, Younger Dryas).

Time BP (ka)	Marine isotope stage	Best estimate (°C)	Minimum envelope (°C)	Maximum envelope (°C)
120	5e	10	8	11
108	5d	-2	-4	0
105	5d	-2	-4	0
102	5c	4	0	8
93	5c	4	0	8
92	5b	-2	-4	0
89	5b	-2	-4	0
85	5a	4	0	10
80	5a	4	0	10
75	4	-4	-8	0
72	4	-4	-8	0
71	4	0	-4	2
68	4	0	-4	2
65	4	-8	-10	-4
60	4	-8	-10	-4
55	3	0	-2	2
50	3	0	-2	2
49	3	-1	-3	2
44	3	-1	-3	2
43	3 (Upton Warren)	6	4	8
42	3	6	4	8
41	3 (Hasselo)	-4	-9	-2
38	3	-4	-9	-2
37.5	3 (Hengelo)	2	0	4
37	3	2	0	4
36	3	-4	-7	-2
32	3	-4	-7	-2
31	3 (Denekamp)	0	-2	4
30	3	0	-2	4
28	3	-4	-6	-2
26	3	-4	-6	-2
25	2	-8	-10	-4
22.5	2	-8	-10	-4
22	2	-5	-8	-4
21.5	2	-5	-8	-4
21	2 (Late Glacial Max.)	-9	-11	-4
19.5	2	-9	-11	-4
19	2	-1	-4	2
18.5	2	-1	-4	2
18	2	-3	-8	-2
17.5	2	-3	-8	-2
16.5	2	-2	-4	2
16	2	-2	-4	2
15.5	2	-4	-8	-2
15	2	-4	-8	-2
14.5	2 (Bölling-Alleröd)	7	4	10
14	2	7	4	10
13	2 (Younger Dryas)	-4	-8	-2

12	2	-4	-8	-2
11.5	1	10	8	11
8	1	10	8	11

3.5.4. Lower boundary condition: geothermal flux

For permafrost modelling the heat capacity, (vertical) thermal conductivity and thermal gradient are essential input parameters to calculate the geothermal flux. In the approach used, these are all dependent on the surface and subsurface temperatures. It should be noted that these thermal properties are regarded as lithological unit specific values, but that they will change as boundary conditions do. For instance, subsurface temperature is modelled using the basal heat flow and surface temperature as main input and will change as surface temperature changes. Gradients, conductivity and heat capacity will vary accordingly.

Heat capacity and thermal conductivity values are given in Table 7 and Table 8. The mid-depth temperature (Table 9) and mid-depth were used, together with surface temperature, to calculate the geothermal gradient (Table 10). Finally, the data are combined to calculate the geothermal flux (Figure 7). Generally speaking, the country is split up between a southeastern part with lower geothermal gradients (0.06-0.07 W/m) and a northwestern part with higher gradients (up to 0.09 W/m). It is interesting to note that this pattern follows the pattern of recent differential tectonic land movement as calculated by Kooi et al. (1998).

For the modelling, the total length of the one-dimensional lithological domain is extended to at least 500 m with clay, in case the overburden does not reach this depth. This implies assuming that the Rupelian layers underlying the overburden are sufficiently thick to bridge the distance from the bottom of the overburden to a depth of 500 m.

Table 7 - Heat capacity (kcal/kg/K). Minimum (min) and maximum (max) values in the dataset are given, as well as the range (Δ), mean, standard deviation (σ) and number of observations.

Polygon	min	max	Δ	mean	σ	n
CNB	0.00	0.21	0.21	0.20	0.03	127529
DRH	0.18	0.20	0.02	0.20	0.00	1384
FPwest	0.19	0.21	0.01	0.21	0.00	2271
FRP	0.13	0.21	0.08	0.20	0.00	56393
GRP	0.01	0.21	0.20	0.20	0.01	105342
KempH	0.04	0.20	0.16	0.20	0.01	1709
LBH	0.01	0.20	0.20	0.19	0.03	4221
LSB	0.16	0.20	0.04	0.20	0.00	30388
NHP	0.18	0.21	0.03	0.21	0.00	16350
OHP	0.20	0.20	0.01	0.20	0.00	15792
PMC	0.07	0.21	0.13	0.20	0.00	42239
PMC zuid	0.14	0.21	0.07	0.20	0.00	3815
RVG	0.18	0.21	0.03	0.21	0.00	46177
TIJH	0.18	0.21	0.02	0.20	0.00	34657
VLB	0.11	0.21	0.10	0.21	0.00	18304
WNB	0.11	0.21	0.10	0.20	0.00	67338
ZH	0.00	0.21	0.21	0.19	0.03	53102

Table 8 – Thermal conductivity (W/m/K). Minimum (min) and maximum (max) values in the dataset are given, as well as the range (Δ), mean, standard deviation (σ) and number of observations.

Polygon	min	max	Δ	mean	σ	n
CNB	0.00	3.30	3.30	2.60	0.47	127529
DRH	2.16	2.70	0.54	2.50	0.08	1384
FPwest	2.94	3.34	0.40	3.07	0.03	2271
FRP	2.52	3.56	1.04	3.06	0.15	56393
GRP	0.14	3.43	3.29	2.70	0.28	105342
KempH	0.59	2.83	2.24	2.36	0.27	1709
LBH	0.07	3.45	3.38	2.67	0.39	4221
LSB	1.93	3.34	1.40	2.67	0.20	30388
NHP	2.78	3.30	0.53	3.00	0.06	16350
OHP	2.03	3.30	1.27	2.66	0.30	15792
PMC	1.03	3.07	2.03	2.54	0.33	42239
PMC zuid	1.86	2.84	0.98	2.79	0.06	3815
RVG	1.71	3.09	1.38	2.74	0.17	46177
TIJH	2.84	3.29	0.45	3.03	0.07	34657
VLB	1.48	3.53	2.06	3.12	0.08	18304
WNB	1.50	3.36	1.87	3.03	0.18	67338
ZH	0.00	4.04	4.04	2.73	0.49	53102

Table 9 - Mid-depth temperature ($^{\circ}\text{C}$). Minimum (min) and maximum (max) values in the dataset are given, as well as the range (Δ), mean, standard deviation (σ) and number of observations.

Polygon	min	max	Δ	mean	σ	n
CNB	10.0	27.8	17.8	18.8	4.7	127529
DRH	11.8	13.4	1.6	12.4	0.4	1384
FPwest	15.5	20.4	4.9	19.6	0.6	2271
FRP	10.3	21.6	11.4	17.4	1.2	56393
GRP	10.0	22.2	12.2	15.0	2.2	105342
KempH	10.5	17.4	6.9	15.2	1.3	1709
LBH	10.0	21.1	11.1	12.2	3.6	4221
LSB	10.4	16.5	6.0	12.6	0.8	30388
NHP	14.6	24.8	10.2	20.9	1.6	16350
OHP	10.6	17.7	7.2	14.5	0.9	15792
PMC	10.0	24.5	14.5	15.3	2.4	42239
PMC zuid	10.0	23.2	13.2	14.7	2.0	3815
RVG	10.4	30.1	19.7	22.9	4.0	46177
TIJH	14.3	22.1	7.7	18.7	0.9	34657
VLB	15.2	26.3	11.1	19.7	0.8	18304
WNB	12.4	24.9	12.6	17.1	2.5	67338
ZH	10.1	16.7	6.6	12.3	0.9	53103

Table 10 – Geothermal gradient (°C/km). Minimum (min) and maximum (max) values in the dataset are given, as well as the range (Δ), mean, standard deviation (σ) and number of observations.

Polygon	min	max	Δ	mean	σ	n
CNB	22.0	32.7	10.7	27.7	2.6	127392
DRH	22.0	28.0	6.0	25.7	1.2	1384
FPwest	26.1	28.5	2.4	27.6	0.4	2258
FRP	25.5	35.1	9.6	28.4	1.4	56258
GRP	22.0	40.9	18.9	28.3	2.9	104959
KempH	23.9	29.2	5.2	26.5	0.6	1707
LBH	22.0	28.0	6.0	23.0	1.6	4164
LSB	22.0	32.2	10.2	24.0	1.3	30366
NHP	24.5	31.4	6.9	28.7	1.6	16268
OHP	23.7	30.1	6.4	26.8	1.2	15792
PMC	22.1	33.9	11.8	27.8	2.2	42218
PMC zuid	22.0	28.0	6.0	25.2	0.9	3792
RVG	22.4	31.1	8.7	27.0	1.6	46166
TIJH	23.5	29.6	6.0	26.9	1.1	34568
VLB	26.9	31.4	4.5	28.8	1.0	18196
WNB	22.9	31.1	8.2	26.4	1.6	67125
ZH	22.4	50.0	27.6	27.2	2.4	52754

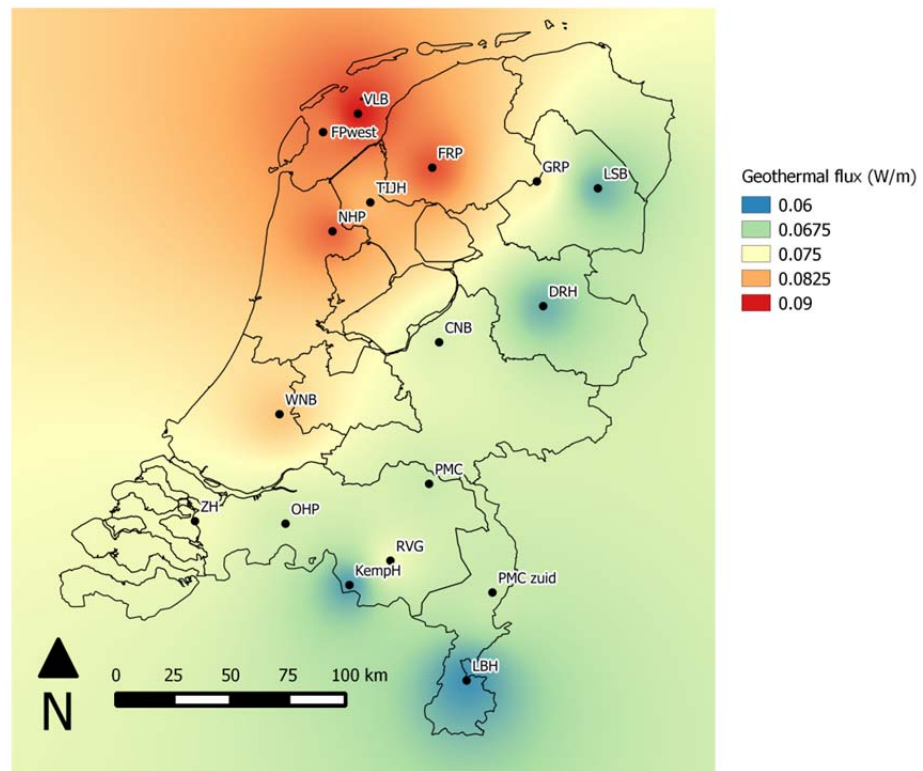


Figure 7 – Geothermal flux (W/m), which is significantly higher in the (north)west than the (south)east of the country.

4. Stochastic uncertainty and sensitivity analysis

4.1. Classification of uncertainties

The goal of a safety case for a final repository project is to prove that the facility will be safe in every respect. This comprises considerations about the near and far future. It is a principal fact, however, that statements about the future can never be more than likelihood statements. Although, by this reason, a strong proof of safety is principally impossible, the remaining uncertainty can be assessed and should be kept as small as possible. This has to be done by carefully identifying and quantifying the primary uncertainties that can have an influence on the overall uncertainty of the safety statement and properly assessing this influence.

As an integral part of a safety case file, supporting calculations for radioactive waste disposal often involves the analysis of complex systems. Various types of uncertainty affect the results of the evaluations carried out in the frame of a performance assessment.

The nature of the uncertainty can be stochastic (or aleatory) or subjective (or epistemic). Epistemic uncertainty derives from a lack of knowledge about the adequate value for a parameter/input/quantity that is assumed to be constant throughout model analysis. In contrast, a stochastic model will not produce the same output when repeated with the same inputs because of inherent randomness in the behavior of the system. This type of uncertainty is termed aleatory or stochastic.

In general a distinction is made between three sources of uncertainty:

- uncertainty in scenario descriptions, including the evolution of the main components of the repository system;
- uncertainty in conceptual models;
- uncertainty in parameter values.

Although both types and even sources of uncertainties cannot be entirely separated, the work in this report deals mostly with subjective (or epistemic) uncertainties which are reflected in the uncertainties in parameter values.

The study of parameter uncertainty is usually subdivided into two closely related activities referred to here as uncertainty analysis and sensitivity analysis, where (i) uncertainty analysis (UA) involves the determination of the uncertainty in analysis results that derives from uncertainty in analysis input parameters and (ii) sensitivity analysis (SA) involves the determination of relationships between the uncertainty in analysis results and the uncertainty in individual analysis input parameters. Sensitivity analysis identifies the parameters for which the greatest reduction in uncertainty or variation in model output can be obtained if the correct value of this parameter could be determined more precisely.

In this work a numerical model, used for the estimation of the permafrost depth across the Netherlands during a Weichselian temperature cycle is evaluated in terms of uncertainty and parameter sensitivity.

4.2. Uncertainty Analysis (UA)

Input factors for most mathematical models consist of parameters and initial conditions for independent and dependent model variables. As mentioned, these are not always known with a sufficient degree of certainty because of natural variation, error in measurements, or simply a lack of current techniques to measure them. The purpose of UA is to quantify the degree of confidence in the existing parameter estimates. In this section we describe the most popular sampling-based approaches used to perform UA, Monte Carlo (MC) methods, and their most efficient implementation, namely the Latin Hypercube Sampling (LHS) technique.

4.2.1. Monte Carlo simulation using Latin Hypercube Sampling

MC methods are popular algorithms for solving various kinds of computational problems. They include any technique of statistical sampling employed to approximate solutions to quantitative problems. An MC simulation is based on performing multiple model evaluations using random or pseudo-random numbers to sample from probability distributions of model inputs. The results of these evaluations can be used to both determine the uncertainty in model output and perform SA. For each parameter, sampling is guided by the specification of a probability density function (pdf) (i.e., normal, uniform, lognormal, triangular, etc.), depending on a priori information. If there are no or little a priori data, a natural choice is a uniform distribution (assigning some hypothetical, but large range with minimum and maximum values for the parameters). If knowledge exists suggesting a more frequent or expected value for a parameter, a triangular or normal pdf would be the best choice (setting the bounding values or variance of the distribution as large as needed). It must be noted that in safety assessments a pdf is seen as a measure of the state of knowledge (or degree of belief).

Several sampling strategies can be implemented to perform UA/SA, such as random sampling, importance sampling, or LHS which is by far the most popular sampling scheme for UA/SA. LHS allows an un-biased estimate of the average model output, with the advantage that it requires fewer samples than simple random sampling to achieve the same accuracy. In LHS, the random parameter distributions are divided into N equal probability intervals, which are then sampled. N represents the sample size. The choice for N should be at least $k+1$, where k is the number of parameters varied, but usually much larger to ensure accuracy. If the interval of variation for some parameter is very large (several orders of magnitude), the sampling can be performed on a log scale to prevent under-sampling in the outer ranges of the interval where the parameter assumes very small values

The latin hypercube sampling is done by randomly selecting values from each pdf. Each interval for each parameter is sampled exactly once (without replacement), so that the entire range for each parameter is explored (Figure 8A). A matrix is generated (which we call the LHS matrix) that consists of N rows for the number of simulations (sample size) and of k columns corresponding to the number of varied parameters (Figure 8B). N model solutions are then simulated, using each combination of parameter values (each row of the LHS matrix). The model output of interest is collected for each model simulation. Different model outputs can be studied if more than one model output is of interest. Monte Carlo Sampling based methods allow performing SA and UA on the same sample.

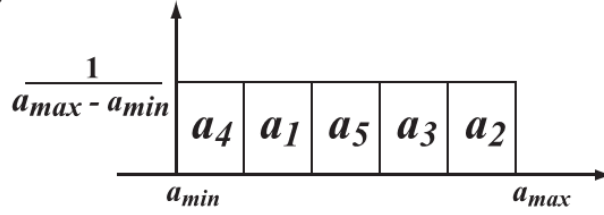
A

$$\begin{array}{ll}
 \text{Mathematical model} & \text{Output} \\
 \dot{\mathbf{x}} = g(\mathbf{x}, \boldsymbol{\theta}), \mathbf{x} \in \mathbb{R}^2 & \longrightarrow y = f(\mathbf{x}; \boldsymbol{\theta}) \\
 \boldsymbol{\theta} \in \mathbb{R}^3, \boldsymbol{\theta} \equiv \{a, b, c\} &
 \end{array}$$

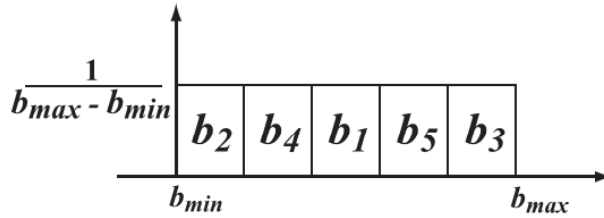
Latin Hypercube Sampling - LHS
Uniform and Normal pdfs

Sample size N=5

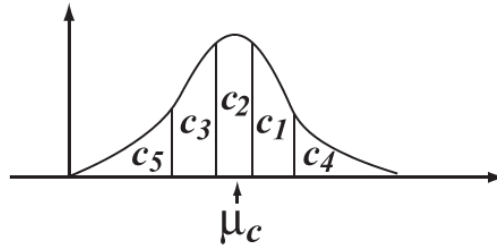
$$a \sim \text{Unif}(a_{\min}, a_{\max})$$



$$b \sim \text{Unif}(b_{\min}, b_{\max})$$



$$c \sim \text{Normal}(\mu_c, \sigma_c)$$



B

LHS MATRIX

OUTPUT MATRIX

$$X = \begin{bmatrix} a_1 & b_1 & c_1 \\ a_2 & b_2 & c_2 \\ a_3 & b_3 & c_3 \\ a_4 & b_4 & c_4 \\ a_5 & b_5 & c_5 \end{bmatrix} \longrightarrow Y = \begin{bmatrix} y_1 = f(a_1, b_1, c_1) = 5.2 \\ y_2 = f(a_2, b_2, c_2) = 7.9 \\ y_3 = f(a_3, b_3, c_3) = 3.1 \\ y_4 = f(a_4, b_4, c_4) = 6.4 \\ y_5 = f(a_5, b_5, c_5) = 0.8 \end{bmatrix}$$

Figure 8: Scheme of uncertainty and sensitivity analysis performed with LHS and regression-based methods. The mathematical model is represented as an ordinary differential equation system, where \mathbf{x} is the vector of state variables in an n -dimensional space \mathbb{R}^n : (as an example we set $n = 2$ and \mathbf{h} is the parameter vector in \mathbb{R}^k ($k = 3$ in this example)). For ease of notation, the output y is unidimensional and it is a function of \mathbf{x} and $\boldsymbol{\theta}$. (A) Mathematical model specification (dynamical system, parameters, output) and the corresponding LHS scheme. Probability density functions (pdfs) are assigned to the parameters of the model (e.g. a, b, c). We show an example with sample size N equal to 5. Each interval is divided into five equiprobable subintervals, and independent samples are drawn from each pdf (uniform and normal). The subscript represents the sampling sequence. (B) The LHS matrix (X) is then built by assembling the samples from each pdf. Each row of the LHS matrix represents a unique combination of parameter values sampled without replacement. The hypothetical model is then solved, the corresponding output generated, and stored in the matrix Y . The LHS matrix (X) and the output matrix (Y) are used to calculate the standardized regression coefficient (SRC) and the partial correlation coefficient (PCC).

4.2.2. Implementation

The calculations are done in three steps, using a Matlab 2012a (Matlab, 2012) linked to the finite element PDE solver Comsol 3.5a.

- First, values of all selected stochastic input variables are sampled for all the runs using in-built Matlab functions. If a correlation is indeed thought to exist between two selected variables, the user can input the wished correlation coefficient value to the program and the sampling will be performed accordingly. This feature was not used as all variables are assumed to be independent.
- A number of simulations are then performed using the sampled parameter combinations. Matlab was used to automate the simulations performed by the FE code COMSOL for all Monte Carlo runs.
- The tables of collected results are produced by Matlab can then be directly analysed with Matlab to calculate and plot the percentiles and mean value of the permafrost depth as a function of time. Then again Matlab was used to compute e.g. Standardized or Partial Correlation Coefficients to investigate the parameter sensitivity.

For the regression based analyses, 1000 realizations are performed to obtain the results for each scenario. In order to guaranty stability of the output, enough number of realizations should be provided. The minimum number of realizations required to assure stable output depends on the system itself and the number of uncertain variables associated with it. In this work, a number of 1000 realizations should be deemed appropriate given the calculation time of one model run. Helton et al. (2005) proved that 100-300 model runs were sufficient for stable results using a complex two-phase flow model with 37 uncertain variables.

4.2.3. Parameter Ranges

The stochastic simulations will give an indication of the probability of nation-wide permafrost depths under a future glacial climate, taking into account various combinations of temperature, overburden lithology, porosity and geothermal flux. The parameters that are investigated in the stochastic analysis are shown in Table 11. Their minimum, maximum en mode values are used to build a triangular probability density functions which are sampled in the stochastic analysis. T1 to T26 are variables which are used to control the magnitude of the various temperature plateaus during the Weichselian temperature cycle. This allows to account for the actual parameter uncertainty as well as the nation-wide spatial parameter variability.

Table 11 – Parameters and associated ranges used in the global UA and SA.

Parameter	Minimum	Maximum	Mode
Porosity [-]	0,2	0,7	0,45
Fraction of sand [-]	0,1	1	0,75
Geothermal flux [W/(m s ²)]	0,033	0,115	0,060
Overburden thickness [m]	20	1500	500
Initial Temperature gradient [K/m]	0,022	0,033	0,028

T1 [K]	281,15	284,15	283,15
T2 [K]	269,15	273,15	271,15
T3 [K]	273,15	281,15	277,15
T4 [K]	269,15	273,15	271,15
T5 [K]	273,15	283,15	277,15
T6 [K]	265,15	273,15	269,15
T7 [K]	269,15	275,15	273,15
T8 [K]	263,15	269,15	265,15
T9 [K]	271,15	275,15	273,15
T10 [K]	270,15	275,15	272,15
T11 [K]	277,15	281,15	279,15
T12 [K]	264,15	271,15	269,15
T13 [K]	273,15	277,15	275,15
T14 [K]	266,15	271,15	269,15
T15 [K]	271,15	277,15	273,15
T16 [K]	267,15	271,15	269,15
T17 [K]	263,15	269,15	265,15
T18 [K]	265,15	269,15	268,15
T19 [K]	262,15	269,15	264,15
T20 [K]	269,15	275,15	272,15
T21 [K]	265,15	271,15	270,15
T22 [K]	269,15	275,15	271,15
T23 [K]	265,15	271,15	269,15
T24 [K]	277,15	283,15	280,15
T25 [K]	265,15	271,15	269,15
T26 [K]	281,15	284,15	283,15

4.3. Sensitivity analysis

A wide range of SA methods exist but can generally be classified into Local and Global techniques. Local SA will be assessing the response of the model output to a small perturbation of single parameters (the so called one at a time method) around a nominal value. The main disadvantage of this method (and other local SA methods) is that information about the sensitivity is only valid for this very specific location in the parameter space only, which is usually not representative of the physically possible parameter space, which becomes problematic especially in the case of non-linear models. To deal with this problem global SA methods have been developed, where multiple locations in the physically possible parameter space are evaluated at the same time. The most frequently used global techniques are implemented using Monte Carlo simulations and are therefore called sampling-based methods. Global SA with regression-based methods rests on the estimation of linear models between parameters and model output. For linear trends, linear relationship measures that work well are the Pearson correlation coefficient (CC), partial correlation coefficients (PCCs), and standardized regression coefficients (SRC). For nonlinear but monotonic relationships between outputs and inputs, the most reliable sampling-based indexes are based on rank transforms such as Spearman rank correlation coefficient (SRCC) and partial rank correlation coefficient (PRCC).

4.3.1. Standardized Regression Coefficients

A sensitivity measure of a model can be obtained using a multiple regression to fit the input data to a theoretical equation that could produce the output data with as small error as possible. The most common technique of regression in sensitivity analysis is that of least squares linear regression. Thus the objective is to fit the input data to a linear equation ($\hat{Y} = aX + b$) approximating the output Y , with the criterion that the sum of the squared difference between the line and the data points in Y is minimized. A linear regression model of the $N \times k$ input sample X to the output Y takes the form

$$Y_i = \beta_0 + \sum_{j=1}^k \beta_j X_{ij} + \varepsilon_i, \quad (5)$$

where β_i are regression coefficients to be determined and ε_i is the error due to the approximation, i.e. $\varepsilon_i = Y_i - \hat{Y}_i$

A measure of the extent to which the regression model can match the observed data is called the model coefficient of determination, R^2 , which is defined as:

$$R^2 = \frac{\sum_{i=1}^N (\hat{Y}_i - \bar{Y})^2}{\sum_{i=1}^N (Y_i - \bar{Y})^2}, \quad (6)$$

where \hat{Y}_i is the approximated output obtained from the regression model and Y_i and \bar{Y}_i are the original values and their mean respectively. If R^2 is close to 1, then the regression model is accounting for most of the variability in Y . A value of R^2 close to 1 indicates that the regression model is accounting for most of the uncertainty in y , while a value of R^2 close to 0 indicates that the regression model do not explain the uncertainty in y , and the model is behaving in a non-linear way.

The regression coefficients β_j , $j = 1, \dots, k$, measure the linear relationship between the input factors and the output. Their sign indicates whether the output increases (positive coefficient) or decreases (negative coefficient) as the corresponding input factor increases. Since the coefficients are dependent on the units in which X and Y are expressed, the normalized form of the regression model is used in sensitivity analysis.

$$\frac{\hat{Y}_i - \bar{Y}_i}{\hat{s}} = \sum_{j=1}^k \frac{\beta_j \hat{s}_j}{\hat{s}} \frac{X_{ij} - \bar{X}_j}{\hat{s}_j}, \quad (7)$$

Where

$$\hat{s} = \left[\sum_{i=1}^N \frac{(Y_i - \bar{Y})^2}{N-1} \right]^{1/2}, \quad \hat{s}_j = \left[\sum_{i=1}^N \frac{(X_{ij} - \bar{X}_j)^2}{N-1} \right]^{1/2} \quad (8)$$

The standardized coefficients $\beta_j \hat{s}_j / \hat{s}$ in Eq.(7), called standardized regression coefficients (SRCs), are used as a sensitivity measure. If X_j are independent, SRCs provide a measure of the importance, based on the effect of moving each variable away from its expected value by a fixed fraction of its standard deviation while retaining all other variables at their expected values. Calculating SRCs is equivalent to performing the regression analysis with the input and output variables normalized to mean zero and standard deviation one.

4.3.2. Correlation coefficients

The Correlation coefficients (CC) usually known as Pearson's product moment correlation coefficients, provide a measure of the strength of the linear relationship between two variables. CC between two N-dimensional vectors x and y is defined by:

$$\rho_{xy} = \frac{\sum_{k=1}^N (x_k - \bar{x})(y_k - \bar{y})}{\left[\sum_{k=1}^N (x_k - \bar{x})^2\right]^{1/2} \left[\sum_{k=1}^N (y_k - \bar{y})^2\right]^{1/2}}, \quad (9)$$

CC only measures the linear relationship between two variables without considering the effect that other possible variables might have. So when more than one input factor is under consideration, as it usually is, partial correlation coefficients (PCCs) can be used instead to provide a measure of the linear relationships between two variables when all linear effects of other variables are removed. The PCC between x_j and y is the CC between the two residuals $X_i - \hat{X}_i$ with the following linear regression models:

$$\hat{X}_i = c_0 + \sum_{j=1, j \neq i}^k c_j X_j, \quad \hat{Y} = b_0 + \sum_{j=1, j \neq i}^k b_j X_j. \quad (10)$$

PCC characterizes the strength of the linear relationship between two variables after a correction has been made for the linear effects of the other variables in the analysis. SRC on the other hand characterizes the effect on the output variable that results from perturbing an input variable by a fixed fraction of its standard deviation. Thus, PCC and SRC provide related, but not identical, measures of the variable importance. When input factors are uncorrelated, PCC and SRC give the same ranking of variable importance.

5. Results

5.1. Permafrost development during a Weichselian temperature cycle – reference case

The permafrost progradation fronts (= location where the temperature reaches 0 °C and the soil is 50% frozen) have been calculated for each of the 17 polygons. Comparable patterns are obtained for the permafrost propagation front in function of time for all polygons. Therefore, as an example, only the results for the FRP and LBH polygons are shown herein function of time (Figure 9 and Figure 10). The permafrost front penetrates about 150 m to 180 m into the subsoil depending on the location, as a result of extremely low mean annual air temperatures during the final phase of MIS4 (early Pleniglacial) and the middle part of MIS2 (late Pleniglacial). Note that maximum permafrost development occurs after the thermal minimum for the cold phase around 60 ka BP. The spatial variability of the maximum depths is discussed in the next section.

We compare the results to other permafrost depth modelling results for NW Europe during the Last Glacial Maximum (LGM, around 20 ka BP) from Delisle (1998), Grassmann et al. (2010), Govaerts et al. (2011) and Kitover et al. (2013). These four different modelling exercises revealed quite contrasting permafrost depths for the LGM, which is not surprising given different approaches and parameter values were used with respect to glacial temperatures, duration of cold phases, thermal sediment properties, heat flux, etc. The values derived from these 4 different studies range between ~ 100 m and ~ 300 m for a western European context, being site or non-site specific. The largest value is from Kitover et al. (2013) who used an extended cold period of unknown duration and a MAAT of -8°C to produce stable permafrost. The lowest value is from Delisle et al. (1998) who used a relatively high MAAT of -7°C for the LGM, a temperature which was reached only during an infinitesimal small time period at around 18 ka according to that study. Furthermore, this study uses the highest geothermal heat flux, 60 mW/m², as is the case for the study by Govaerts et al. (2011). The latter however used a lower MAAT (-9°C) for the LGM, persisting for 2000 years and preceded by already very cold temperatures in the millennia before. Depending on the type of vegetation and the presence or absence of snow, permafrost depths between 200-250 m were calculated (Govaerts et al., 2011). Similar values were obtained in the study by Grassman et al. (2010) for northern Germany.

The shallower permafrost depths calculated in the present study compared to Govaerts et al. (2011) in which the same model was used, can be attributed to the much higher porosity values of the overburden (40-50% compared to 30%).

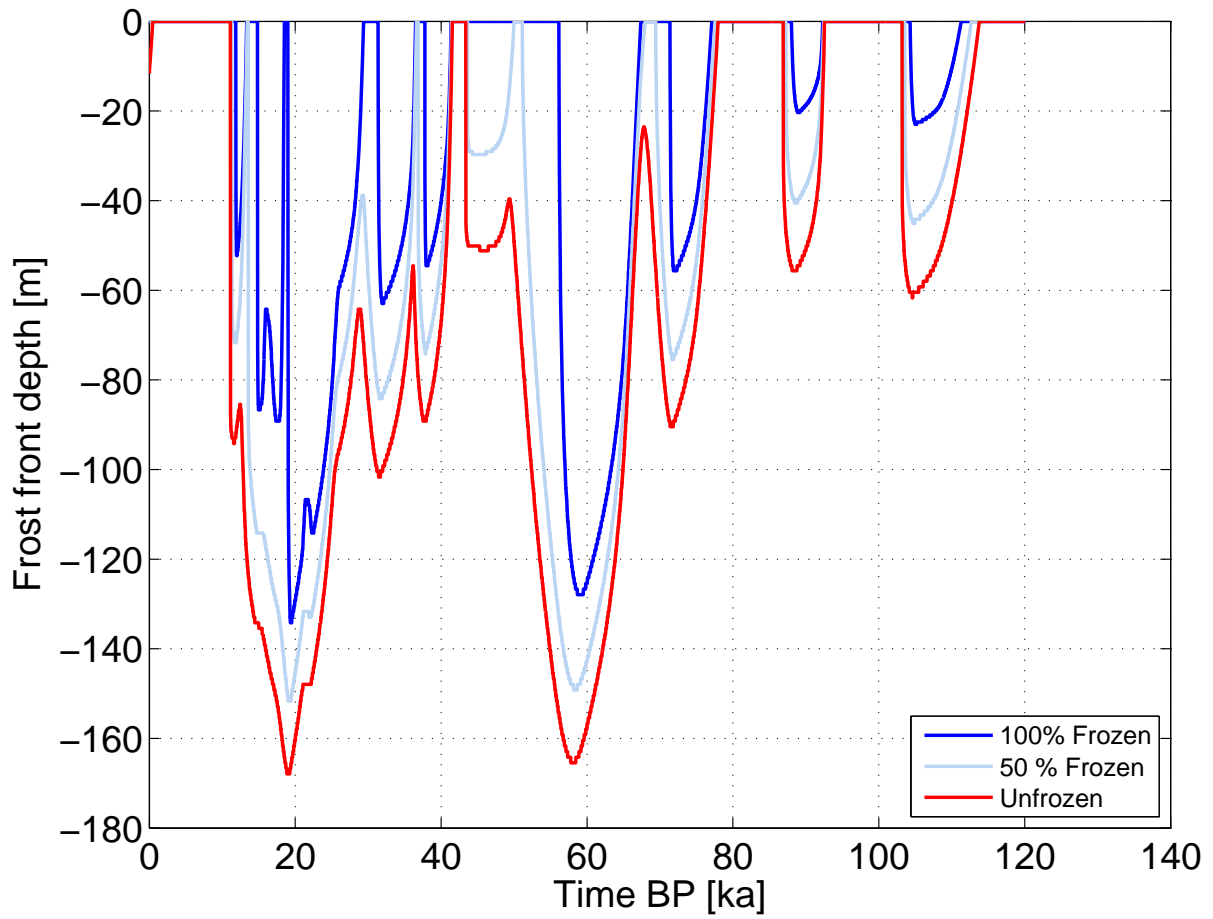


Figure 9: Permafrost progradation during a simulation of the Weichselian glaciation cycle for the FRP polygon

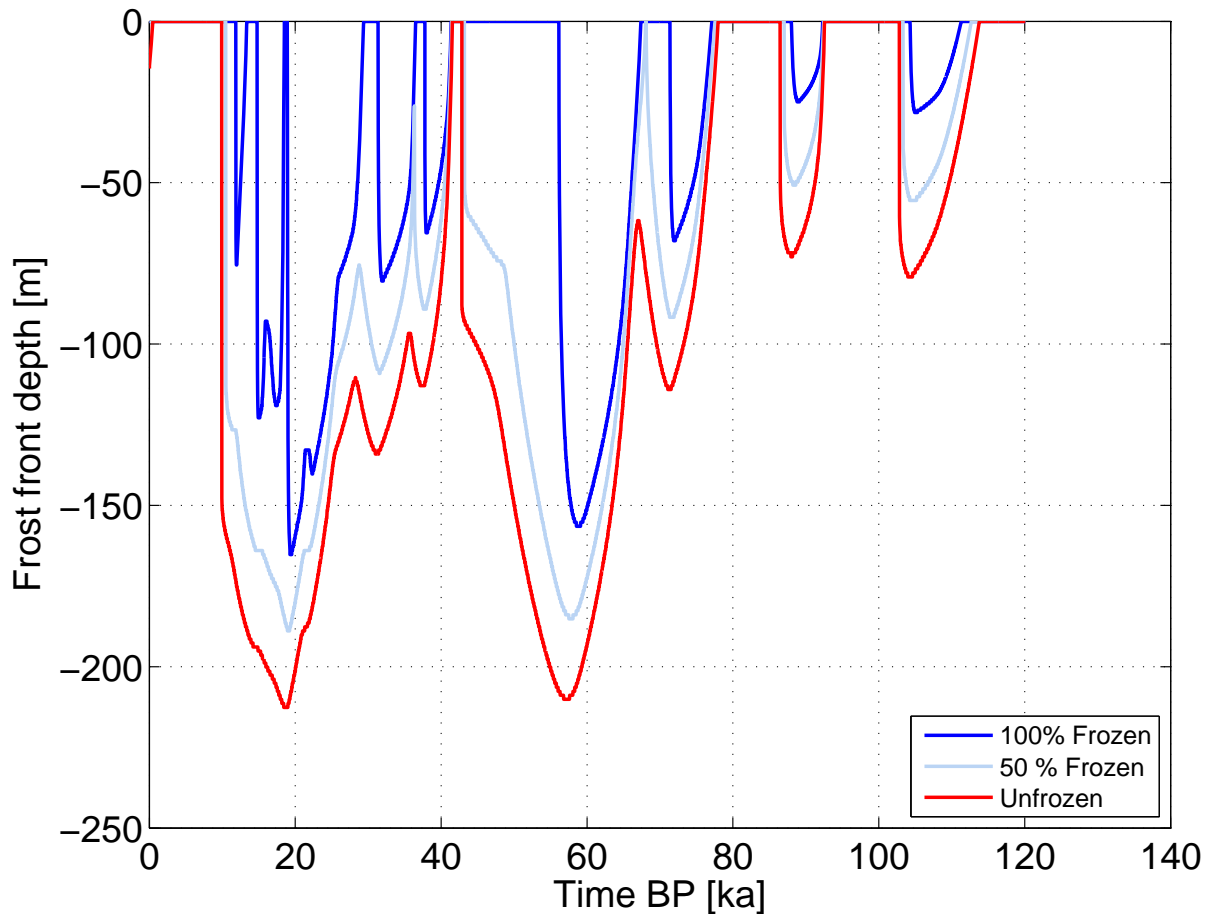


Figure 10: Permafrost progradation during a simulation of the Weichselian glaciation cycle for the LBH polygon

5.2. Interpolated best estimate maximum permafrost depth maps - reference case

The spatial distribution of maximum permafrost depth at any time during a Weichselian climatic analogue is given in Figure 11, Figure 12 and Figure 13 for various freezing levels. The maps are interpolated (inverse distance weighted) from individual polygon results, and are the result of model forcing by the best estimate climate evolution given in Figure 1. The maximum permafrost depth generally corresponds with the coldest peak in MIS2 (around 20 ka BP). For the state in which all pore water is in the liquid phase ('unfrozen' i.e. the 0.5°C isotherm), maximum depth ranges between 210 m in the southeast and 170 m in the northwest of the Netherlands (Figure 11). Similar patterns can be observed for 50% and 100% frozen iso-line (Figure 12 and Figure 13). The spatial variability in permafrost depth is further illustrated along a N-S transect, from polygon centre FRP in the north to LBH in the south (Figure 14).

Somewhat surprisingly, the calculated permafrost depth would be about 40 m less in the north. Intuitively, one would expect permafrost to reach greater depths in the north, because of the inferred colder temperatures in the north of the country. However, as stated above, the input temperature was kept constant for the entire study area, such that the results can be interpreted solely in terms of subsurface properties. The spatial pattern of maximum permafrost depth is in fair

agreement with the pattern of geothermal flux, as shown in Figure 7, and a relationship with the weight fraction of sand can be observed as well (Figure 2). This seems logical as a higher geothermal flux imposes a stronger resistance against the intrusion of subzero temperatures into the soil. A higher sand fraction facilitates permafrost growth, as a sand matrix has a higher thermal conductivity which allows a more rapid extraction of thermal energy towards the surface during cold periods.

Thus, assuming a constant temperature evolution over the Netherlands, geothermal fluxes, and to a lesser extent sand percentage, seem to be the determining factor to explain the N-S variability of the maximum permafrost depth. Parameter sensitivity will be addressed in more detail in the section on the sensitivity analysis.

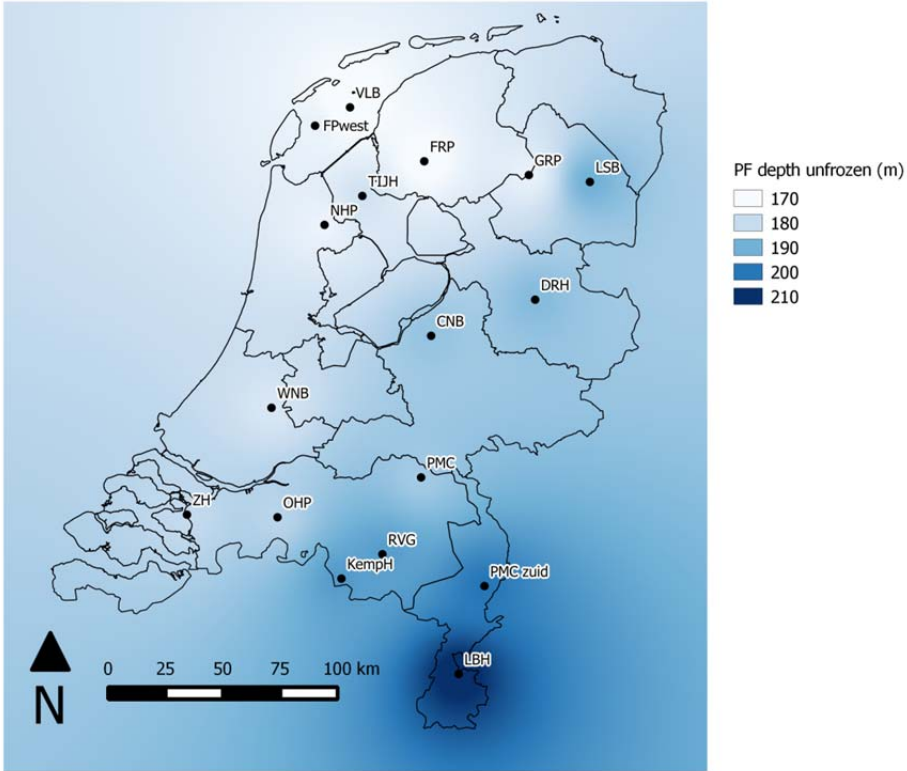


Figure 11 – Interpolated best estimate maximum permafrost depth map for the +0.5°C isotherm, that is the point at which the freezing process starts. Below this depth, all pore water is in the liquid phase.

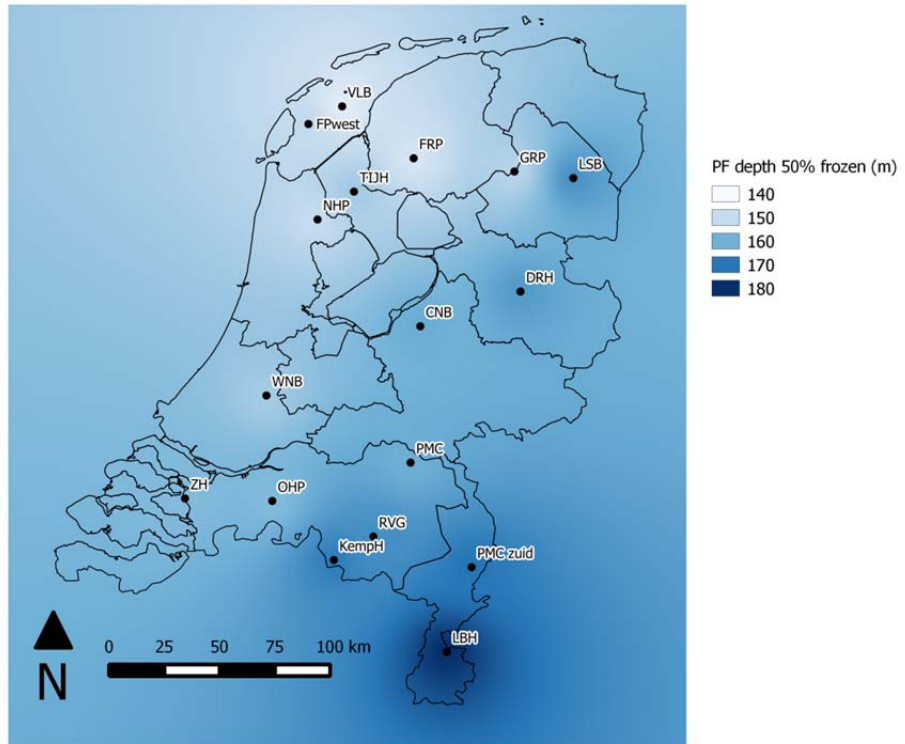


Figure 12 – Interpolated best estimate maximum permafrost depth map for the 0°C isotherm. Fifty percent of the pore water along this contour map is in the liquid phase.

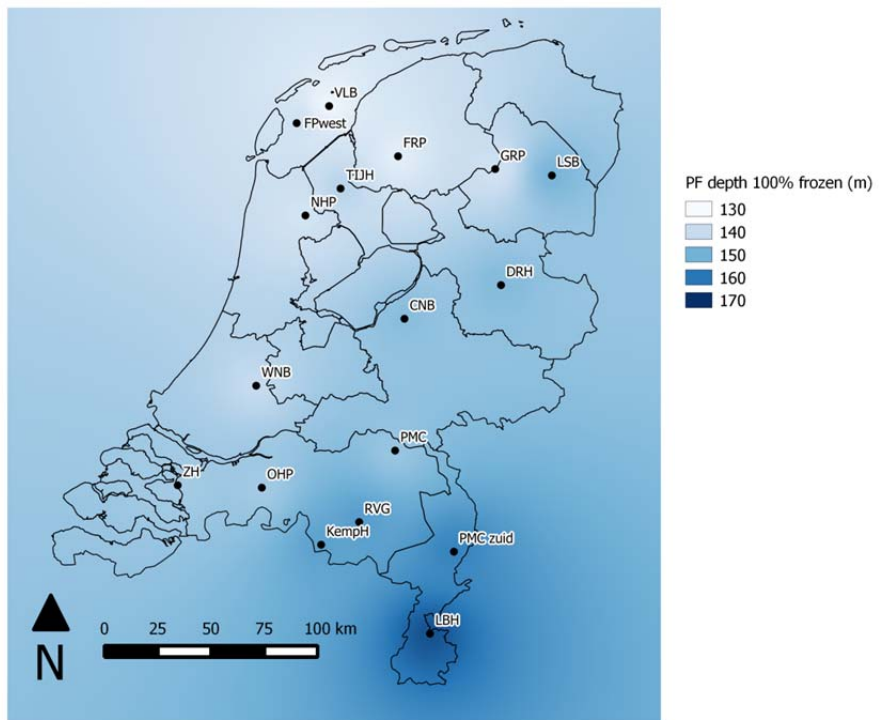


Figure 13 – Interpolated best estimate maximum permafrost depth map for the -0.5°C isotherm. Above this depth, all pore water is frozen.

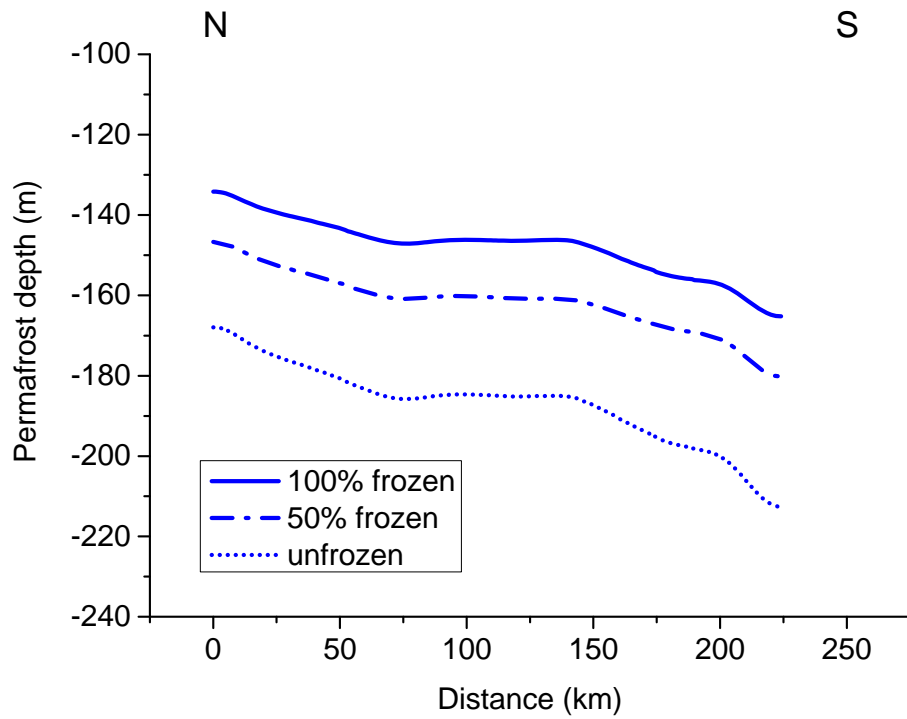


Figure 14 – Permafrost depth for different freezing states along a N-S transect from polygon centre FRP in the north to LBH in the south.

Table 12: Maximum permafrost depth per polygon and for different freezing states.

Polygon	PF depth unfrozen (m)	PF depth 50% frozen (m)	PF depth 100% frozen (m)
CNB	186	161	147
DRH	188	164	148
FPwest	173	151	138
FRP	168	147	134
GRP	173	152	138
KempH	194	169	153
LBH	213	180	165
LSB	190	165	149
NHP	172	150	137
OHP	181	158	144
PMC	184	160	145
PMC zuid	200	170	158
RVG	193	166	153
TIJH	178	154	142
VLB	165	144	132
WNB	176	154	140
ZH	180	158	144

5.3. Results of the uncertainty analysis

The uncertainty analysis translates the uncertainty on the input parameters into an uncertainty on the permafrost depth (= 50% frozen isoline). The results are shown in [Figure 15](#) and [Figure 16](#). The concurrency of the mean value and the 50-percentile indicates that the model behaves linearly. The mean and median values of the maximum permafrost depth at a time of 20 ka BP are about 150 m, while the most conservative parameter combinations result in permafrost fronts going as deep as 270 m.

The difference between the 5% and 95%-percentiles (2σ) is about 80 m, which is a relatively large interval given the low number of parameters. It is recommended to diminish the uncertainty on a number of important parameters in future analyses of permafrost evolution.

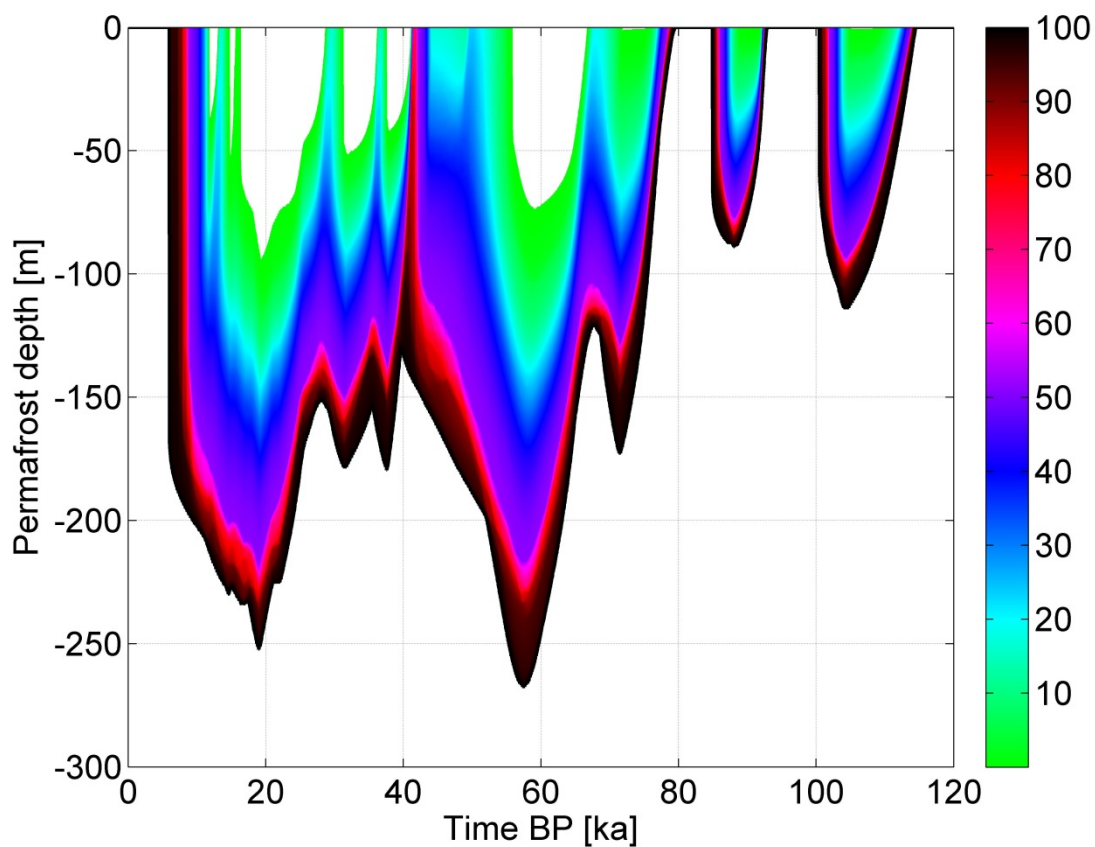


Figure 15: All percentiles of permafrost front penetration during a stochastic nation-wide simulation of the Weichselian glaciation

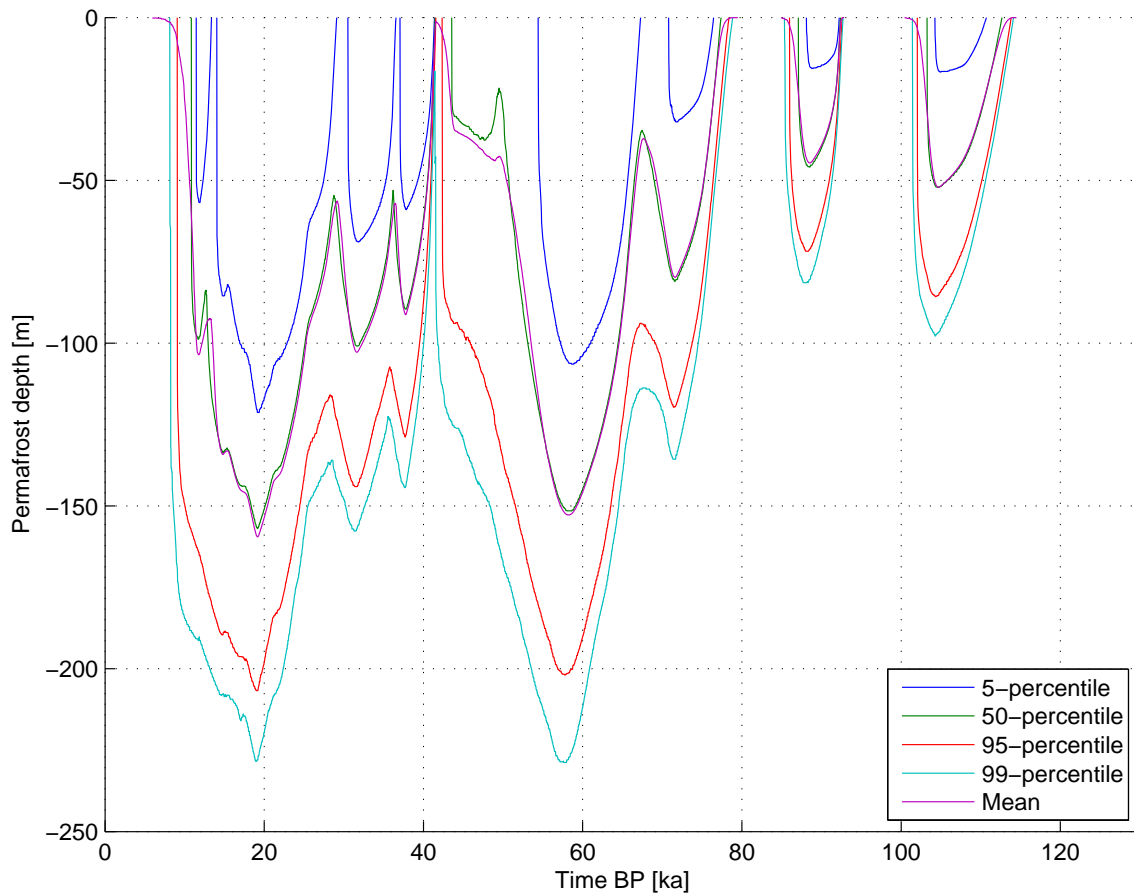


Figure 16: Selected percentiles and mean values of permafrost front penetration during a stochastic nation-wide simulation of the Weichselian glaciation

5.4. Results of the sensitivity analysis

The goal of the sensitivity analysis (SA) is to determine the relationships between the uncertainty in output and the uncertainty in individual input parameters. SA identifies the parameters for which the greatest reduction in uncertainty or variation in model output can be obtained if the correct value of this parameter could be determined more precisely. The results are analysed by looking at the evolution of the standardized regression coefficients (SRC) and partial correlation coefficients (PCC). PCC and SRC provide related, but not identical, measures of the variable importance. If input factors are independent, PCC and SRC give the same ranking of variable importance. A positive correlation coefficient (SRC/PCC) means that a higher value of the parameter will cause a larger permafrost depth and vice versa. Figures 17 – 20 show the time evolution of the correlation coefficients.

It can be seen in Figure 17 that the R^2 -values are close to 1, this indicates that the regression model is accounting for most of the uncertainty in the permafrost depth, and the model is behaving in a linear way.

Both the PCC and SRC indicate that the geothermal flux is the most important parameter. It is interesting to note that during permafrost growth (e.g. around 90 ka BP), the geothermal flux is

equally important as the porosity. When the surface temperature again rises and the permafrost starts to degrade, the geothermal flux acts as the main driving force of the melting process.

During the course of simulation time, correlation coefficients can change their sign. During permafrost growth, at the initial phase of a subzero temperature period, a higher porosity will decrease permafrost growth. A larger pore water content means that a larger amount of energy needs to be removed from the subsoil in order to cool it down, because of the larger effective heat capacity, and to induce a phase change of the total amount of pore water. A larger water content also decreases the total effective thermal conductivity which slows down the extraction of thermal energy towards the surface. Thereafter, during the subsequent warmer period, a higher ice content will require a larger amount of heat to be supplied to melt away the permafrost.

The sand fraction shows a relatively strong, positive influence on permafrost depth which confirms the findings of the nationwide simulation. Compared to clay, sand has a higher thermal conductivity which cause a more rapid cooling of the subsurface during cold periods.

The overburden thickness only seems to be an important parameter during the early, moderately cold periods, when the MAAT is slightly below zero (e.g. MIS 5b and 5d). For the modelling, the total length of the one-dimensional lithological domain is extended to at least 500 m with clay, in case the overburden does not reach this depth. Clay has a lower thermal conductivity than the (mostly) sandy overburden, and this will decrease the maximum permafrost depth. Furthermore, a larger overburden will increase the domain size, thus imposing the geothermal flux at a larger distance from the top. The effect of the overburden seems to be the most important in the early cold periods when the surface temperature is slightly below the freezing point. In these periods the permafrost front will not penetrate strongly into the underground and the location of the clay/sand interface will have a severe impact on the retardation of the temperature wave. In extremely cold periods like the final phase of MIS4 (early Pleniglacial) and the middle part of MIS2 (late Pleniglacial), the temperature at the surface is low enough to push the freezing front sufficiently deep in order to render the exact depth of the clay/sand interface rather superfluous. Therefore, the other parameters become gradually more important as the simulation progresses in time.

Finally, it is no surprise that, being the driving force for the formation of a permafrost, the surface temperature is very important at the time it is imposed at the top of the computational domain (Figure 20). It is key to note that a specific correlation coefficient becomes larger when that temperature is maintained for a longer period. Closer to the present, the dynamics of the temperature evolution during the Weichselian are better captured in the proxy data, which translates itself to a more detailed temperature evolution in the 50 – 0 ka BP timeframe. Subsequently, this makes the individual temperature parameters seem less important compared to the early temperatures, which can be seen as an artefact induced by the dynamics of the temperature curve.

Another interesting point to note is the fact that a cold temperature during an early timeframe can still manifest its influence thousands of years later. For instance, the PCC-curves of T6 and T7 show a long tailing as they still impact the formation of the permafrost around 60 ka BP. This can be explained by the thermal inertia of the frozen soil, which has not been fully reverted to the initial temperatures at the start of a subsequent cold period.

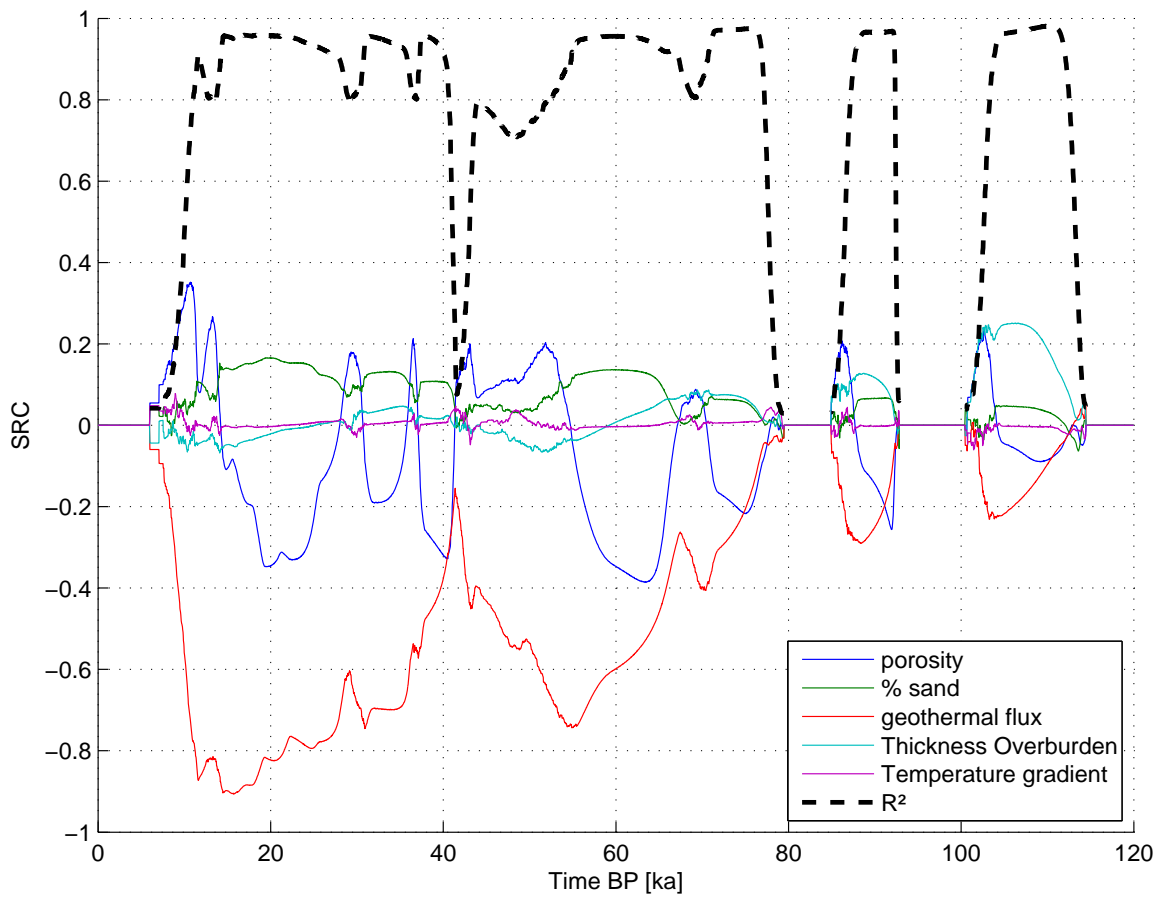


Figure 17: Time evolution of the SRCs for the physical parameters of a permafrost progradation simulation during a Weichselian glaciation.

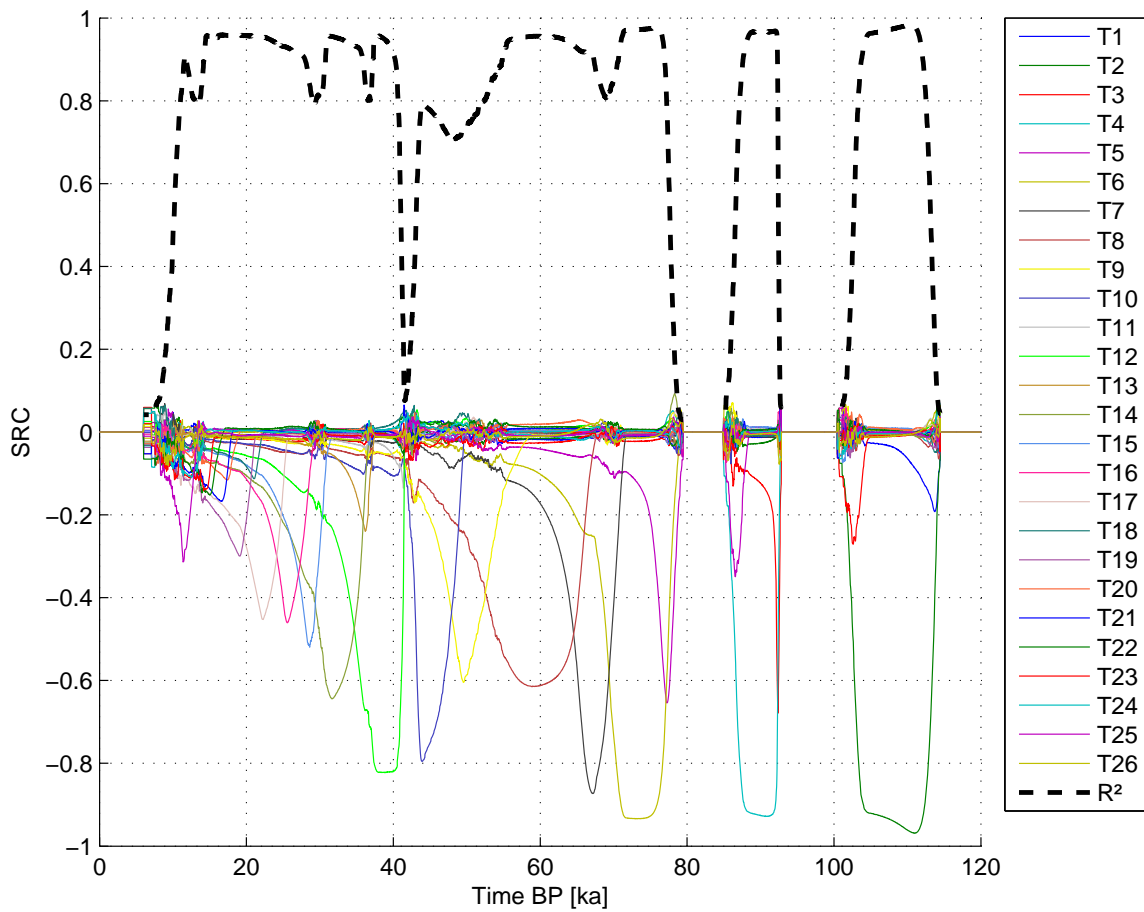


Figure 18: Time evolution of the SRCs for the imposed surface temperatures of a permafrost progradation simulation during a Weichselian glaciation.

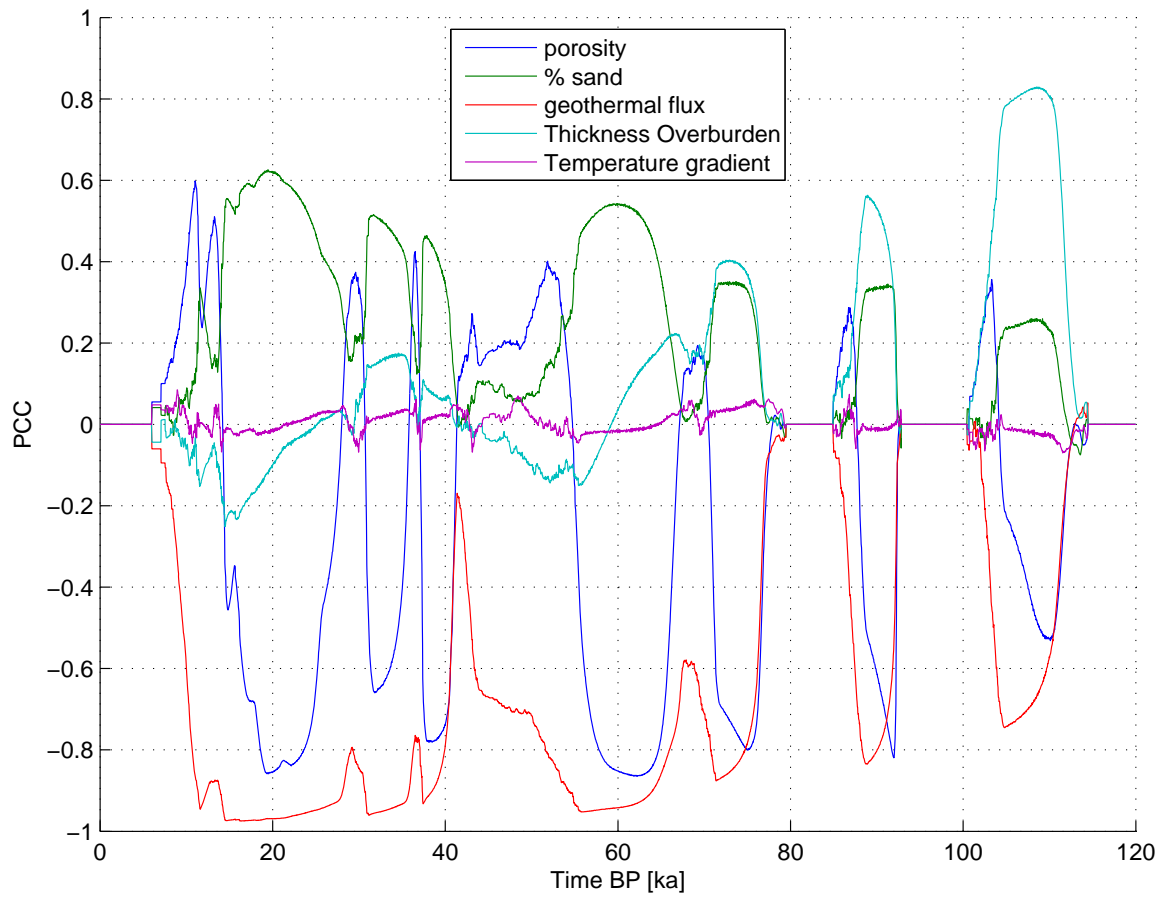


Figure 19: Time evolution of the PCCs for the physical parameters of a permafrost progradation simulation during a Weichselian glaciation.

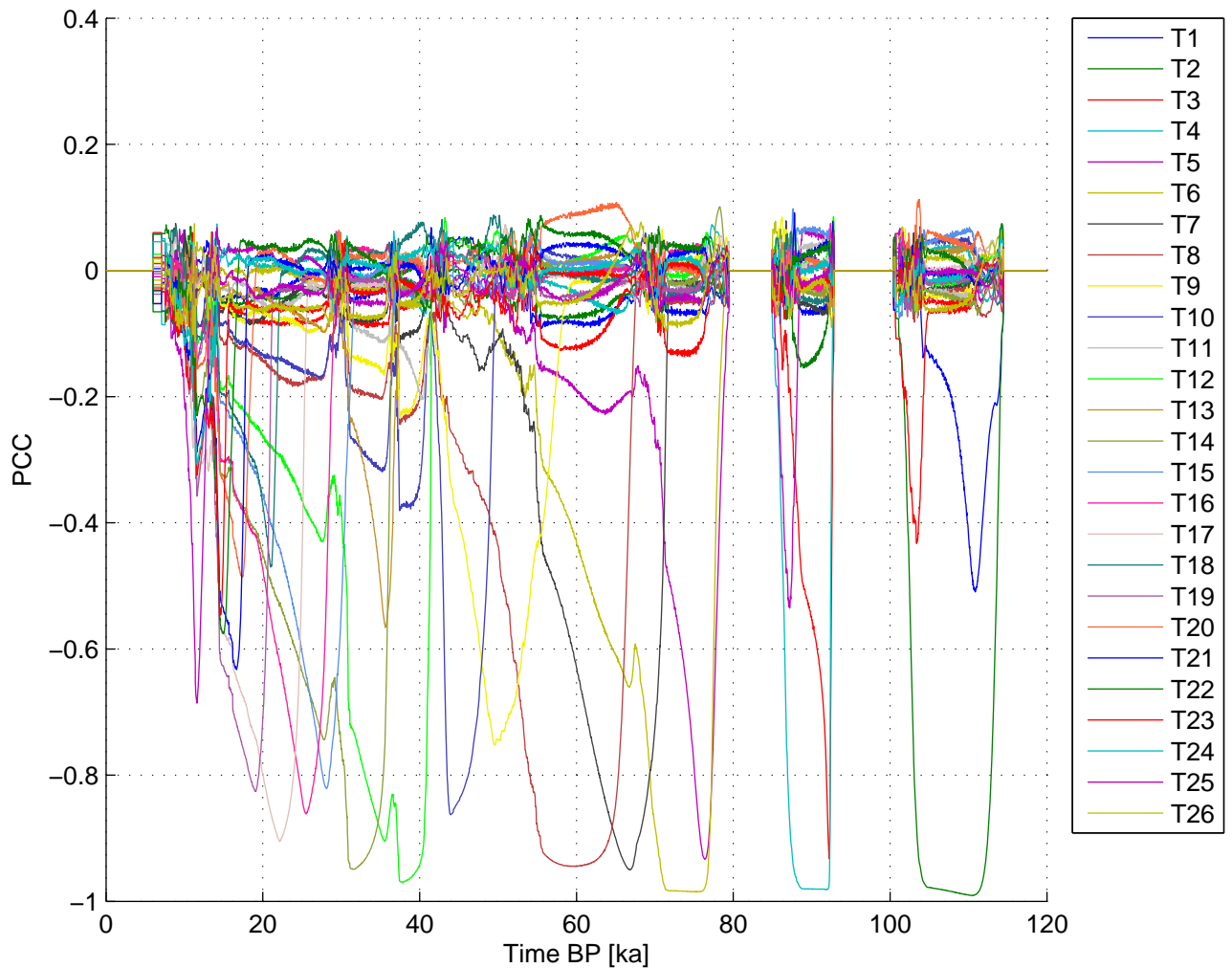


Figure 20: Time evolution of the PCCs for the imposed surface temperatures of a permafrost progradation simulation during a Weichselian glaciation.

6. Conclusions

Permafrost depth modelling using a best estimate temperature curve of the Weichselian as an analogue for the future indicates that the permafrost front (50% ice and 50% water) would indicate permafrost depths between 140-180 m in the Netherlands. Using the same climatic data for the entire country, deepest permafrost is expected in the south, due to the lower geothermal flux and higher average sand content of the post-Rupelian overburden. Taking into account various sources of uncertainty, such as type and impact of vegetation, snow, air surface temperature gradients across the country, possible errors in palaeoclimate reconstructions, porosity, lithology and geothermal flux, stochastic calculations point out that permafrost depth during the coldest stages of a glacial cycle such as the Weichselian, for any location in the Netherlands, would be between 120-200 m at the 2 σ level. In any case, permafrost would not reach depths greater than 270 m. The most sensitive parameters in permafrost development are the mean annual air temperatures and porosity, while the geothermal flux is the crucial parameter in permafrost degradation once temperatures start rising again.

The calculations presented here are robust and conservative. However, in order to further reduce existing uncertainties, the following phenomena should be taken into account: the effect of groundwater flow on permafrost development, the effect of salt content on freezing temperatures, vegetation and snow cover and a realistic temperature gradient over the Netherlands.

7. References

Beerten, K., 2011, Permafrost in northwestern Europe during the Last Glacial, External Report of the Belgian Nuclear Research Centre, Mol, Belgium, SCK•CEN-ER-138.

Bense, V.F., Ferguson, G., Kooi, H., 2009. Evolution of shallow groundwater flow systems in areas of degrading permafrost. *Geophysical Research Letters*, 36.

BIOCLIM, 2001. Deliverable D3: Global climatic features over the next million years and recommendation for specific situations to be considered. Modelling Sequential Biosphere Systems under Climate Change for Radioactive Waste Disposal. A project within the European Commission 5th Euratom Framework Programme Contract FIKW-CT-2000-00024s. <http://www.andra.fr/bioclim/documentation.htm>

Busschers, F.S., Kasse, C., van Balen, R.T., Vandenberghe, J., Cohen, K.M., Weerts, H.J.T., Wallinga, J., Johns, C., Cleveringa, P., Bunnik, F.P.M., 2007. Late Pleistocene evolution of the Rhine-Meuse system in the southern North Sea basin: imprints of climate change, sea-level oscillation and glacio-isostasy. *Quaternary Science Reviews* 26, 3216-3248.

Buylaert, J. P., Ghysels, G., Murray, A. S., Thomsen, K. J., Vandenberghe, D., De Corte, F., Heyse, I., Van den haute, P., 2008. Optical dating of relict sand wedges and composite-wedge pseudomorphs in Flanders, Belgium. *Boreas* 38, 160–175.

Chen G., Sillen X., Verstricht J., Li X.- Revisiting a simple in situ heater test: the third life of ATLAS.- Clays in Natural and Engineered Barriers for Radioactive Waste Confinement.- Nantes, France, 29 March - 1 April 2010.

COMSOL, 2008. COMSOL Multiphysics 3.5a, Earth Science Module, COMSOL AB, Stockholm, Sweden.

Delisle, G., 1998. Numerical simulation of permafrost growth and decay. *Journal of Quaternary Science* 13, 325-333.

Helton J.C., Davis, F.J., Johnson, J.D., 2005, A comparison of uncertainty and sensitivity analysis results obtained with random and Latin hypercube sampling. *Reliability Engineering and System Safety* 89, 305–330

Govaerts, J., Weetjens, E., Beerten, K., 2011. Numerical simulation of permafrost depth at the Mol site. External Report SCK•CEN-ER-148.

Guiot, J., Pons, A., De Beaulieu, J.L., Reille, M., 1989. A 140,000-year continental climate reconstruction from two European pollen records. *Nature* 338, 309–313.

Grassmann, S., Cramer, B., Delisle, G., Hantschel, T., Messner, J., Winsemann, J., 2010. pT-effects of Pleistocene glacial periods on permafrost, gas hydrate stability zones and reservoir of the Mittelplate oil field, northern Germany. *Marine and Petroleum Geology* 27, 298-306.

Hartikainen, J., 2006. Numerical Simulation of Permafrost Depth at Olkiluoto. Posiva 2006-52.

Holmén, J., H. Benabderrahmane, A. Buoro, and J. Brulhet, 2011, "Modelling of Permafrost Freezing and Melting and the Impact of a Climatic Cycle on Groundwater Flow at the Meuse/Haute-Marne Site," *Physics and Chemistry of the Earth*, Vol. 36, Nos. 17–18, pp. 1,531–1,538.

Kitover, D.T., van Balen, R.T., Roche, D.M., Vandenberghe, J., Renssen, H., 2013. New Estimates of Permafrost Evolution during the Last 21 k Years in Eurasia using Numerical Modelling. *Periglacial Processes and Landforms* 24, 286–303.

Kooi, H., Johnston, P., Lambeck, K., Smither, C., Molendijk, R., 1998. Geological causes of recent (~ 100 yr) vertical land movement in the Netherlands. *Tectonophysics* 299, 297–316.

Kömle N.I., Bing H., Feng W.J., Wawrzaszek R., Hütter E.S., He Ping, Marczewski W., Dabrowski B., Schröer K., Spohn T., 2007. Thermal conductivity measurements of road construction materials in frozen and unfrozen state. *Acta Geotechnica* 2, 127–138.

Lunardini, V. J., 1978. Theory of n-factors and correlation of data. In *Proceedings of the 3rd International Conference on Permafrost*, 10–13 July 1978, Edmonton, Alta. National Research Council of Canada, Ottawa, Ont., 1, 40–46.

Mallants, D., 2006. Basic concepts of water flow, solute transport, and heat flow in soils and sediments, second edition. SCK•CEN-BLG-991, 169-183.

Marivoet, J., Bonne, A., 1988, PAGIS, disposal in clay formations, SCK•CEN-R-2748

Matlab, 2012, The MathWorks. <http://www.mathworks.com/>

Mottaghy, D., Rath, V., 2006. Latent heat effects in subsurface heat transport modelling and their impact on palaeotemperature reconstructions. *International Journal of Geophysics* 164, 236–245.

NGRIP – North Greenland Ice Core Project members,

22, 209-223.

van Gijssel, K., 1995. A 2004. High-resolution record of Northern Hemisphere climate extending into the last interglacial period. *Nature* 431, 147–151.

Noetzli, J., Gruber, S., 2009. Transient thermal effects in Alpine permafrost. *The Cryosphere* 3, 85–99.

Renssen, H., Vandenberghe, J., 2003. Investigation of the relationship between permafrost distribution in NW Europe and extensive winter sea-ice cover in the North Atlantic Ocean during the cold phases of the Last Glaciation. *Quaternary Science Reviews hydrogeological and palaeoenvironmental data set for large-scale groundwater flow model simulations in the northeastern Netherlands*. *Meded. Rijks Geol. Dienst* 52, 105-134.